गेहूँ में फसल वृद्धि का छायाचित्र आधारित लक्षणप्ररुपण

IMAGE BASED PHENOTYPING OF CROP GROWTH IN WHEAT

MAHESH MEENA

Roll. No. 20591

DIVISION OF PLANT PHYSIOLOGY

ICAR-INDIAN AGRICULTURAL RESEARCH INSTITUTE

NEW DELHI-110012

2016

IMAGE BASED PHENOTYPING OF CROP GROWTH IN WHEAT

BY

MAHESH MEENA

A Thesis

Submitted to the Faculty of Post-Graduate School,
ICAR-Indian Agricultural Research Institute, New Delhi
In partial fulfillment of requirements for the award of the degree of

MASTER OF SCIENCE

IN

PLANT PHYSIOLOGY

NEW DELHI

2016

Approved by:

Chairman	:	Dr. Rakesh Pandey	_____
Co-chairman	:	Dr. Vijay Paul	_____
Members	:	Dr. Viswanathan Chinnusamy	_____
		Dr. Pramod Kumar	_____
		Dr. Archana Singh	_____
		Dr. Neelu Jain	_____

Division of Plant Physiology
ICAR-Indian Agricultural Research Institute
New Delhi -110012

Dr. Rakesh Pandey
Principal Scientist

CERTIFICATE

This is to certify that the thesis entitled "**IMAGE BASED PHENOTYPING OF CROP GROWTH IN WHEAT**" submitted to the Faculty of the Post-Graduate School, ICAR-Indian Agricultural Research Institute, New Delhi, in partial fulfillment of **MASTER OF SCIENCE** in **PLANT PHYSIOLOGY**, embodies the results of bonafide research work carried out by **Mr. MAHESH MEENA**, under my guidance and supervision, and that no part of this thesis has been submitted for any other degree or diploma.

The assistance and help availed during the course of investigation as well as source of information have been duly acknowledged by him.

Date:

Place: New Delhi

Dr. RAKESH PANDEY
Chairman
Advisory committee

ACKNOWLEDGEMENTS

As a prelude to my thanks giving, at first I wish to thank the ***Nature*** *for giving me strength, courage and confidence…after all she is the "Greatest".*

Though only my name appears on the cover of this thesis, a great many people have contributed to its production. I owe my gratitude to all those individuals who have made this thesis possible and because of whom my experience has been one that I will cherish forever.

I wish to express my deepest sense of gratitude and indebtedness to ***Dr. Rakesh Pandey, Principal Scientist,*** *ICAR - Indian Agricultural Research Institute, New Delhi and Chairperson of my Advisory Committee for his invaluable guidance, constant encouragement, untiring enthusiasm, affectionate behaviour, and peerless criticism during the course of investigation and preparation of manuscript. He was always there in all my needs and helped his best whenever I sought it. His kindness and devotion left an indelible impression in my mind.*

I am deeply indebted to ***Dr. Vijay Paul,*** *Co-chairman of my Advisory committee, Division of Plant Physiology and,* ***Dr. Viswanathan Chinnusamy****, Principal Scientist and Head, Division of Plant Physiology,* ***Dr. Pramod Kumar****, Senior Scientist, Division of Plant Physiology,* ***Dr. Archana Singh,*** *Senior Scientist, Division of Biochemistry and* ***Dr. Neelu Jain,*** *Senior Scientist, Division of Genetics, member of my Advisory Committee for their critical comments, valuable suggestions, guidance and help in research work and analysis.*

My sincere thanks are due to ***Dr. C. Vishwanathan,*** *Head, Division of Plant Physiology,* ***Dr. V.P. Singh****, Professor, Division of Plant Physiology, for providing me the necessary facilities throughout the study.*

I also express my gratitude to all the faculty members for their guidance. I also thank to Mrs. Sunita Sharma, PA to Professor for helping and monitoring our PG activities throughout the entire M.Sc. tenure.

I owe a lot to my friends Gautam, Indrajeet, Abhilash, Alka, Sachidanand, Ashok, Ajay, Taklu, PN sharma ji for all kinds of moral support and affection.

Candid thanks to all my seniors, especially Shiva rama sir, Krishna sir, Shivani mam, Deepika mam, Ankit sir, Madhurima mam, Surendra sir, Abhisek sir, Scientist (IIRS-ISRO), Naveen gupta sir, Gajendra sir, mukesh sir, Vicky sir, Priyanka mam, Soumya mam, Milan sir, Suprokash sir, Rajeev sir, Vasundhara mam and Prabha mam who helped me throughout this period of studentship at IARI, New Delhi. I am also extraordinarily fortunate to have generous and helpful juniors Sandeep, Adhip, Elongavan. I am thankful to my batchmates ***Nitin, Lakshmi*** *and* ***Shamima*** *for their friendly approach and moral support throughout my entire M.Sc. tenure.*

I convey my thanks to ***Shri Tirtha Dasgupta Sir*** *of* ***Central Photo Lab, IARI, Harikrishna sir, Division of Genetics*** *and staff of Division of Plant Physiology IARI, New Delhi for their help rendered during laboratory work. I am thankful to Dr. Sitaram sir, R.C. Meena sir, Banerjee sir, Umesh Thakur ji, Chandreshwar ji, Bhupen ji and other supporting staff for their help and support.*

The endless love, affection, sacrifice and constant inspiration from my ***Parents, my Bros, Sis, my Mamaji*** *and* ***Laddu*** *who have boosted my moral and self esteem and saved me through the thick and thin of my course of study. I owe a lot to them.*

Finally, the financial assistance provided by the Indian Council of Agricultural Research, New Delhi in the form of ***ICAR-Junior Research Fellowship*** *during the tenure is gratefully acknowledged.*

Place: New Delhi

Date: ***(Mahesh Meena)***

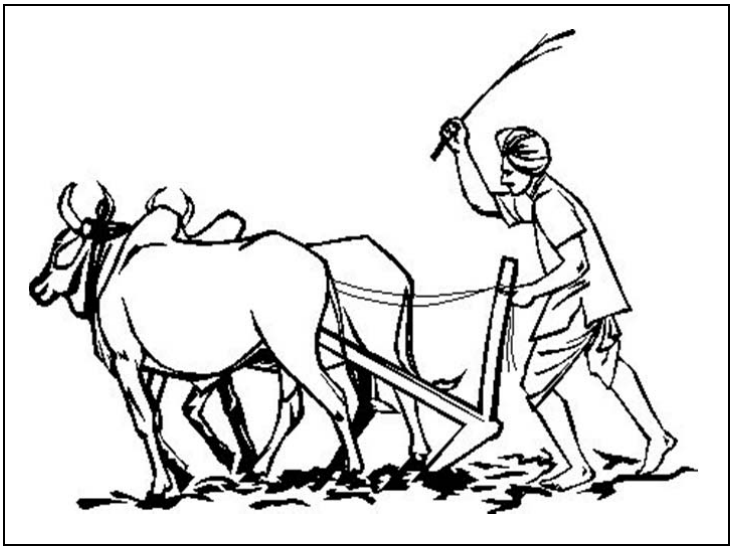

जल, जंगल, जमीन एवं अन्नदाता

को समर्पित

CONTENTS

LIST OF TABLES

LIST OF FIGURES

LIST OF PLATES

Chapter 1

INTRODUCTION

One of the most important representative traits of crop performance is biomass production. The biomass production directly shows the plants ability to grow and is associated with crop growth, yield, Harvest Index (HI), Radiation Use Efficiency (RUE), Water Use Efficiency (WUE), Nutrient Use Efficiency (NUE), fodder availability, carbon capture etc. Yield is product of crop biomass and harvest index. As harvest index of wheat is approaching ceiling, further increases in yield potential will require enhancing the biomass (Sharma Natu and Ghildiyal 2005, Hawkesford *et al.* 2013, Reynolds *et al.* 2012). Crop growth represents increase in biomass and leaf area and it is one of the most important representative traits of crop performance. Better canopy growth in term of biomass accumulation and leaf area production is visible through extent of ground cover (Mullan and Reynolds, 2010). Estimation of biomass and canopy growth by traditional method requires destructive sampling, more time, expenses and labour. It is therefore highly desirable that biomass can be measured rapidly, non-destructively and precisely so that high breeding efficiency is achieved for crop improvement through conventional, molecular or transgenic approaches (Araus and Cairns 2014). Therefore, there is need for developing non-destructive and rapid methods for field phenotyping using image based techniques.

High throughput phenotyping involves the use of visible, infrared, thermal, LiDAR, laser based scanners and other sensors along with software for image processing and analysis. For this purpose, there is availability of high throughput automated plant phenotyping platforms under controlled conditions. In general these are highly efficient systems in terms of precision and throughput but are expensive due to the type of hardware required for robotics, conveyor belts, cameras, computing infrastructure and greenhouse conditions (Fiorani and Schurr 2013). Leister *et al.* (1999) were the first to study plant growth in *Arabidopsis thaliana* by non-invasive image analysis under controlled environment. Top view of plant trays were used for plant area estimation. Fresh weight and plant area were correlated. Tackenberg (2007) studied biomass, growth rates, vertical biomass distribution and dry matter content using scaled digital images under controlled greenhouse in twenty-seven annual and

perennial grass species (Poaceae). Projected area and the proportion of greenish pixels were calculated. They observed a high correlation between log-log relation of dry matter and projected area. Golzarian *et al.* (2011) estimated shoot biomass of cereal plants from their two dimensional images as a linear function of the projected shoot area of plants in the images. However estimation of crop biomass under field conditions in terms of faster and non-destructive approaches is still difficult and there is need to study this aspect.

Under field conditions, the most widely used image based method involves capture of top view of the canopy for non-destructive and rapid phenotyping of canopy cover and biomass (Mullan and Reynolds 2010). However, the method is not suitable after full ground cover by the canopy. Another useful approach involves the side view profile of isolated plants (Takenberg 2007). But, there is no imaging method available for capturing sided view images from crop rows under field conditions.

In this context the visible imaging can offer simple solutions due to ready availability of digital cameras. Therefore, the present research work proposal has been formulated to study and develop image based methods for field phenotyping of biomass and crop growth in wheat by capturing side view image profiles from wheat crop rows in field with a new method and apparatus.

The proposed objective of the study is as follows –

Developing rapid and non-destructive image based methods for field phenotyping of biomass and crop growth in wheat.

Chapter 2

REVIEW OF LITERATURE

Image based phenotyping of biomass and canopy growth in plants

Introduction

Plant phenotype represents the observable structural and functional plant characteristics or traits in a given environment. The phenotype includes growth, development, physiology, tolerance to stress, yield etc. and should be selectable for its application in crop improvement. It is highly desirable that particular phenotype can be measured rapidly, non-destructively and precisely so that high breeding efficiency is achieved in conventional, molecular or transgenic approaches (Araus and Cairns 2014). Phenotyping has been defined as the set of methodologies and protocols used to measure a specific trait related to plant structure or function (e.g. plant growth, architecture and composition) with a certain accuracy and precision at different scales of organization, from organs to canopies (Fiorani and Schurr 2013, Ghanem *et al.* 2014, Li *et al.* 2014).

Out of the various plant morphological traits used in phenotyping e.g. plant height, leaf area, architecture, branches and tillers etc., the biomass production is the most important parameter. The biomass production directly shows the plants ability to grow and is associated with yield which is product of crop biomass and harvest index. As harvest index is approaching ceiling, further increases in yield potential will require enhancing the biomass (Sharma Natu and Ghildiyal 2005, Hawkesford *et al.* 2013, Reynolds *et al.* 2012). Crop growth represents increase in biomass and leaf area and it is one of the most important representative trait of crop performance. Better canopy growth in term of biomass accumulation and leaf area production is visible through extent of ground cover (Mullan and Reynolds, 2010). Estimation of canopy growth by traditional method requires destructive sampling for biomass and leaf area. It requires more time, labour and one can't measure any parameter again. During germplasm evaluation experiments a lot of material needs to be compared for physiological traits related to crop growth and stress tolerance. The plants also may be limited and destructive sampling becomes a majar limitation.

The present review describes the different image based methods employed in the non destructive phenotyping of plant biomass and growth parameters under field and controlled conditions. The outline of review with recent advances is as follows –

I. Image based methods of biomass and growth estimation in plants under controlled conditions
II. Image based methods of biomass and growth estimation in plants under field conditions
III. Different platforms for deployment of sensors under field conditions
IV. Ground cover and leaf area index estimation from images

2.1. Image based phenotyping of biomass and growth in plants under controlled conditions

2.1.1. Visible image (RGB) based estimations

RGB images in the controlled conditions are very useful because there are no fluctuating light conditions and also the background can be controlled to a great extent. Moreover, measuring plant growth in the field requires careful note of variables particularly light condition and camera calibration which is not a problem under controlled conditions. Therefore RGB imaging is the basic component of presently available high throughput phenotyping platforms. Some studies depicting the use of RGB images under controlled environments are as follows. Leister *et al.* (1999) were the first to study plant growth in *Arabidopsis thaliana* by non-invasive image analysis under controlled environment. Top view of plant trays were used for plant area estimation. Fresh weight and plant area were correlated. Tackenberg (2007) studied biomass, growth rates, vertical biomass distribution and dry matter content using scaled digital images under controlled greenhouse in twenty-seven annual and perennial grass species (Poaceae). Projected area and the proportion of greenish pixels were calculated. They observed a high correlation between log-log relation of dry matter and projected area. Walter *et al.* (2007) used GROWSCREEN for quantifying the dynamics of seedling growth from images in tobacco and *Arabidopsis thaliana* under controlled environment. Rapid detection of genetic and environmental parameters regulating plant growth was made possible. Golzarian *et al.* (2011) estimated shoot biomass of cereal plants from their two dimensional images as a linear function of the projected shoot area of plants in the images. They proposed a

method based on plant specific weight for improving the accuracy of the linear model and reducing the estimation bias.

2.1.2. Visible, Near-Infrared and Fluorescence image based estimations

The measurement of side view projected areas as done in the earlier approach has been currently complemented with the multiple angle views including top view (Fiorani and Schurr 2013) to measure the digital volume of plant. In these measurements, fluorescence images and near-infrared images were also used in addition to RGB images. The digital volume of plant has been found highly correlated with shoot biomass. Klukas *et al*. (2014) have described a new platform called Integrated Analysis Platform (IAP) which is an open-source framework for high-throughput phenotyping. They validated its performance from maize plants with non-destructive imaging. Using the IAP platform, they compared four different formulas based on the parameters of visible and fluorescence imaging. These formulas were as follows – IAP volume (V_{IAP}), KeyGene volume ($V_{Keygene}$), LemnaTec volume ($V_{LemaTec}$), Prism volume (V_{Prism})

$$V_{IAP} = \sqrt{A_{s.average}^2 \times A_{t.average}}$$

$$V_{LemnaTec} = \sqrt{A_{s.0^\circ} \times A_{s.90^\circ} \times A_t}$$

$$V_{Keygene} = A_{s.0^\circ} + A_{s.90^\circ} + \log\left(\frac{A_t}{3}\right)$$

$$V_{Prism} = \sqrt{\frac{A_t \times A_{s.45^\circ} \times A_{s.90^\circ}}{2}} \sqrt{1 - \left(\frac{A_{s.45^\circ}^2 + A_{s.90^\circ}^2 - A_{s.0^\circ}^2}{2 \times A_{s.45^\circ} \times A_{s.90^\circ}}\right)^2}$$

Where,

A_s = projected areas from side-view

A_t = projected areas from top-view images (at different angles)

$V_{LemnaTec}$ is formula used in the LemnaTec software to estimate plant volume

$V_{Keygene}$ is formula used in the KeyGene

V_{Prism} is formula used in the Prism

It was observed that in general the correlation of fluorescence image based digital volume showed a higher correlation with fresh weight (0.9685-0.9770)

compared to visible image based digital volume (0.9507-0.9637). Similarly, the fluorescence image based digital volume showed a higher correlation with dry weight (0.8994-0.9281) compared to visible image based digital volume (0.8277-0.8370).

Arvidsson *et al.* (2011) described a growth phenotyping pipeline for *Arabidopsis thaliana* with platform Scanalyzer HTS, LemnaTec, Wuerselen, Germany. Phenotypic parameters - area, convex hull and compactness provided quantification of genotype effects with respect to growth. The system was able to phenotype rosette area of 7000 plants/day by RGB image using the parameters of area, convex hull and compactness. The study quantified genotype effects on total rosette area and relative leaf growth rate (RLGR). Berger *et al*. (2012) has provided protocol to estimate biomass and growth assuming relation between biomass and projected area for a growth phenotyping pipeline for *Arabidopsis thaliana* using with platform of LemnaTec 3D Scanalyzer system, Germany. Honsdorf *et al.* (2014) used a high-throughput phenotyping platform (The Plant Accelerator, Australia) equipped with LemnaTec 3D Scanalyzer (LemnaTec, GmbH, Germany) to capture RGB top view image and two side views in barley under controlled environment. A high correlation ($r = 0.98$) was observed between image based biomass estimates and actual biomass. Neilson *et al.* (2015) used a shoot imaging system (The Plant Accelerator, The University of Adelaide, Australia - Scanalyzer 3D imaging system, LemnaTec). A strong positive correlation was found between projected leaf area and above-ground biomass, height, and true leaf area. The RGR output showed significant correlation with the RGR by traditional destructive harvests. Parent *et al.* (2015) used The Plant Accelerator controlled greenhouse facilities (Australia). The plants were imaged using a LemnaTec 3D Scanalyzer to study genetic control of growth and transpiration. The biomass and leaf area were estimated from images and growth rate was calculated. The observed and measured biomass were highly correlated ($P<0.001$). Neumann *et al.* (2015) used a high-throughput genotyping platform (LemnaTec 3D Scanalyzer, Germany) to image top view image side view images for estimation of plant volume in barley under controlled environment. High correlation was observed between destructively measured plant fresh weight and digital biomass ($R^2 > 0.9$).

Chen *et al.* (2014) used a LemnaTec HTS-Scanalyzer 3D platform for dissecting the phenotypic components of crop plant growth and drought responses in barley under controlled environment. Three types of image data - near-infrared (NIR), visible (color), and fluorescence were acquired daily from different views. Phenotypic features (54 nos.) of the drought responses of 18 different barley genotypes were studied and color imaging was used for biomass accumulation and growth. Digital volume showed the best correlation with manually measured fresh weight and dry weight and logistic model simulated biomass accumulation better (r = 0.89). Junker *et al.* (2014) observed significant correlation between fresh biomass and estimated volume of 63 maize inbred lines grown in various growth conditions. Top and side view RGB images, fluorescence signals (FLUOR) and broad band near infrared (NIR) images were taken with the IPK LemnaTec Scanalyzer systems for small and for large plants under controlled environment. Fahlgren *et al.* (2015) phenotyped wild *Setaria viridis* and domesticated *Setaria italica* under controlled-environment. The platform (The LemnaTec Scanalyzer 3D) recorded fluorescence, near-infrared, and visible images to measure biomass and growth rates. Chen *et al.* (2016) predicted barley plant biomass from image-derived parameters using automated phenotyping and imaging platform LemnaTec-Scanalyzer 3D. Plants were phenotyped using visible (or color), fluorescence (FLUO) and near-infrared (NIR) sensors. Plant biomass was accurately predicted from images using a random forest model. Hairmansis *et al.* (2014) used image-based phenotyping for non-destructive screening in rice for salinity tolerance under controlled conditions. The platform was called Plant Accelerator (Australian Plant Phenomics Facility) and images were taken using the LemnaTec 3D Scanalyzer system (Germany). Total shoot area and senescent shoot area, calculated from visible red-green-blue (RGB) and fluorescence images helped in biomass estimation.

Dhondt *et al.* (2014) studied time-resolved imaging of in vitro Arabidopsis rosette growth under controlled environment. Petri dishes were placed on a rotating disk and top view images were taken. Analysis of several growth-related parameters over time in mutants revealed specificities in growth behavior. Humplík *et al.* (2015) made high-throughput phenotyping of plant shoots for study of the cold-tolerance of pea using Plant ScreenTM phenotyping platform (Photon Systems Instruments, Brno, Czech Republic). Digital RGB image analysis helped in correlation between green

area and biomass. Bac-Molenaar *et al.* (2015) used PHENOPSIS phenotyping platform for genome-wide association mapping of growth dynamics in *Arabidopsis* under controlled environment. Rosette growth was measured by top-view imaging. Fresh weight was positively correlated with projected leaf area (PLA) after 14 days (r>0.95). Edlich-Muth *et al.* (2016) worked on phenomic prediction of maize hybrids using automated greenhouse facility (Leibniz Institute of Plant Genetics and Crop Plant Research (IPK), Germany). Twenty image features explained 73% of the variance in hybrid fresh weight. Flood *et al.* (2016) studied growth and reflectance in *Arabidopsis thaliana* using an automated high-throughput phenotyping platform, the Phenovator, capable of screening 1440 Arabidopsis plants multiple times per day at Wageningen University, The Netherlands. Growth rates were estimated from projected leaf area (PLA). Fluctuation in PLA between day and night were captured emphasizing the importance of frequent measurements and change in leaf angle in light and dark. Cabrera-Bosquet *et al.* (2016) studied radiation-use efficiency of thousands of plants in a phenotyping platform using PHENOARCH platform based on a PhenoWareTM system Lyon, France. Leaf area and fresh plant weight of individual plants were estimated from images and a high correlation between biomass accumulation and intercepted PPFD was observed.

2.2. Image based phenotyping of biomass and growth in plants under field conditions

2.2.1. Digital Camera based biomass estimation - Visible images

Earlier workers e.g. Weiner *et al.* (1998) have lamented that "plant ecology suffers from lack of an efficient technology for measuring plant size non-destructively and non-invasively". However, the advent of digital cameras lead to promising solutions for estimation of green biomass, soil cover, plant color etc Casadesus *et al.*. (2007). Paruelo *et al.* (2000) studied above-ground plant biomass using a photographic technique. Photographs of 0.25 m^2 circular plots were taken from a SLR camera mounted 1.4 m above the ground. The percentage of "green pixels" in the digital image and green grass biomass showed a correlation of 0.87. Tomasel *et al.* (2001) studied chromaticity-based technique for estimation of above-ground plant biomass from a short-grass steppe. Quantitative estimates of green or dry biomass were made using colour information from digital pictures which showed high correlation between

pixel count and measured values of green biomass (r = 0.95). Mullan and Reynolds (2010) and Mullan *et al.* (2012) described estimation of digital ground cover (DGC) using color digital camera. The crop ground cover or the percentage of soil surface covered by plant foliage was estimated from images in Photoshop. DGC was related to biomass (R^2 = 0.63). Lee *et al.* (2013) used digital camera image analysis for estimation of rice growth and nitrogen nutrition status. Canopies cover (CC) and ten color indices were calculated from digital camera images and a high correlation was observed between CC and shoot dry weight (0.81). Casadesús and Villegas (2014) estimated leaf area index and biomass using conventional digital cameras. The image derived index pertaining to the fraction of green pixels over the total pixels of the image showed good correlations with all biomass variables and was robust to lighting conditions. Jia *et al.* (2014) used digital images to monitor the growth of cotton crop in field. The green and red values from the digital images were used to estimate canopy cover. The canopy cover and above-ground biomass were closely related (R^2 = 0.74-0.94). Hunt *et al.* (2015) used a custom-made high-throughput image analysis tool for estimation of dry matter production of individual perennial ryegrass in field. The image analysis tool was faster and estimates of plant area were more highly correlated with measured DM values, potentially capturing 25% more of the variation, than those from visual growth scores. Kefauver *et al.* (2015) measured RGB picture vegetation indexes from field grown maize. The RGB picture vegetation indexes outperformed NDVI with R^2 values up to 0.65, compared to 0.56 for NDVI. Hoyos-Villegas *et al.* (2014) used common digital cameras for phenotyping soybean growth and yield. They took weekly digital images of each plot to estimate canopy cover, total above-ground biomass, leaf biomass, photosynthesis, and grain yield. High correlation between the ground cover data (image analysis) and crop growth rate was observed (R^2 = 0.69). Sieling *et al.* (2016) measured dry matter partitioning and canopy traits in wheat and barley using digital pictures under field conditions. Green Area Index (GAI) was estimated from digital pictures. Lootens *et al.* (2016) studied lateral expansion and regrowth of spaced *Lolium perenne* plants using top view images with a DSLR camera. High-throughput phenotyping for image based plant's base area, tiller number, image based regrowth after cutting and leaf growth two weeks after cutting showed r values up to 0.792 and 0.824.

2.2.2. Digital Camera based biomass estimation – Visible and NIR images

Use of both the Visible and NIR images from digital cameras can be helpful in estimation of NDVI which is associated with biomass and crop growth. Recently, Greider *et. al.* (2015) estimated RGR in wheat non-destructively under field conditions using NDVI canopy cover images. Sakamoto *et al.* (2012) used camera observation system called Crop Phenology Recording System (CPRS) for monitoring crop growth of maize and soybean in field. It consisted of two digital cameras for visible and near infrared (NIR) imaging. The camera-derived vegetation indices and the satellite spectral reflectance observations (SKYE and MODIS) were used. The analysis showed that a vegetation index (night time relative brightness index of NIR) was closely associated with total above-ground biomass for both maize and soybean. Dammer *et al.* (2016) made on-the-go phenotyping in field potatoes using camera vision. Measurements of NDVI were made using camera and reflected light under field conditions. The study helped in identifying areas showing different plant growth and differences in the temporal development of the crop. Schirrmann *et al.* (2016) studied wheat biomass by combining image clustering with crop height. They measured Plant coverage percentage, NDVI and NIR images using a multisensory approach combining a digital camera system with an arbitrary crop height measuring platform under field conditions. Clustering yielded more accurate estimates of fresh and dry biomass (R^2 = 0.79/0.68) than NDVI image clustering (R^2 = 0.66/0.56). The combination of image clustering with crop height increased model quality.

2.3. Different platforms for deployment of biomass and growth sensing systems under controlled and field conditions

2.3.1. Automated plant phenotyping platforms for controlled conditions

There are many high throughput plant phenotyping platforms operation under controlled conditions. In general these are highly efficient systems in terms of precision and throughput but are expensive due to the type of hardware required for robotics, conveyor belts, cameras, computing infrastructure and greenhouse conditions (Fiorani and Schurr 2013). Many of the studies reported in literature have been done with the help of commercially available platforms available from LemnaTec Systems, Germany [Arvidsson *et al.* (2011), Berger *et al.* (2012), Honsdorf *et al.* (2014), Neilson *et al.* (2015), Parent *et al.* (2015), Neumann *et al.* (2015), Chen

et al. (2014), Junker *et al.* (2014), Chen *et al*. (2016) and Hairmansis *et al.* (2014)]. It is a highly automated, high throughput plant phenotyping platform (HTPP) which can perform fast imaging in time series under controlled conditions. It can phenotype multiple point plant growth in plants by quantitative area measurement and colour classification. LemnaTec has developed systems for phenotyping individual plants in large, robotic greenhouses. Using technologies combining photography, fluorescence imaging, 3D image analysis, and data handling, thousands of individual plants can be grown and automatically tracked through their development. A conveyor constantly moves potted plants around the greenhouse and through a series of scanning chambers. Studies on other important HTPP are as follows - Humplík *et al.* (2015) used Plant ScreenTM phenotyping platform (Photon Systems Instruments, Brno, Czech Republic). Bac-Molenaar *et al.* (2015) used PHENOPSIS phenotyping platform. Edlich-Muth *et al.* (2016) used automated greenhouse facility (Leibniz Institute of Plant Genetics and Crop Plant Research (IPK), Germany). Flood *et al.* (2016) worked with automated high-throughput phenotyping platform, the Phenovator at Wageningen University, The Netherlands. Cabrera-Bosquet *et al.* (2016) studied radiation-use efficiency of thousands of plants in a phenotyping platform using PHENOARCH platform based on a PhenoWareTM system Lyon, France. To overcome the difficulty in phenotyping taller plants such as tall pepper (over 3m high) which couldn't be transported to imaging chambers, van der Heijden *et al*. (2012) made a new system. The device was equipped with several cameras positioned along the height to capture images upwards at intervals. The set-up could find the three QTLs by image analyses which were earlier observed from manual measurements.

2.3.2. Vehicle based platforms for field (hand trolleys and tractor driven)

The biomass estimation in crops can be done in more efficient and rapid manner by installing the sensors on moving platforms which may be manual driven cart or sensors mounted on tractor. The vehicle based platforms may be normal or multisensor based and such ground based vehicles with GPS navigation devices are also called phenomobiles (Araus and Cairns 2014). An example of manual cart is provided by White and Conley (2013) where they evaluated a low cost cart for crop phenotyping. It consisted of sensors - radiometers and infrared thermometers. Hunt *et al.* (2015) estimated dry matter production of individual perennial ryegrass plants in

field using a custom-made high-throughput image analysis tool. Estimates of plant area were highly correlated with measured dry matter however the accuracy lowered for dry matter above 15 g. Crain *et al*. (2016) developed a low-cost phenotyping platform named Phenocart. It consisted of a GreenSeeker for spectral reflectance, an infrared thermometer (IRT), and a global navigation satellite system (GNSS) receiver. The CT and NDVI were significantly correlated to yield.

One of the tractor operated multisensory platform for non-destructive field-based phenotyping e.g. biomass estimation is Breedvision (Busemeyer *et al.* 2013a, b). It was used for precision phenotyping of biomass accumulation in *Triticale*. BREEDVISION is equipped with two light curtains, three laser distance sensors, two 3D-Time-of-Flight cameras and a hyperspectral imaging system equipped with a 120 W halogen lighting system. It extracts different parameters (Plant height, Penetration-depth-sidewise-3D, Penetration-depth-top-3D, Coverage density) from sensor data. Sensor fusion helped to accurately predict biomass under field conditions (R^2 values of 0.93 and 0.84). Ehlert *et al.* (2003) made a vehicle based mechanical sensor for determination of wheat plant mass under field conditions. Correlation between plant biomass and pendulum angle was observed. Kipp *et al.* (2014) studied early plant vigour of winter wheat using a vehicle based multispectral active sensor and two commercially available active sensors (GreenSeeker and CropCircle). Early Plant Vigor Index (EPVI) was measured. They found that EPVI and the relative amount of green pixels (RAGP) derived from digital images were significantly related to each other (R^2 = 0.98). Erdle *et al.* (2013) studied phenotypic differences in biomass in relation to Water Index (R970/R900) and NIR/NIR-based index (R760/R730). A tractor-based high-throughput canopy reflectance measurement platform was used. They observed good association between biomass and spectral indices. Svensgaard *et al.* (2014) developed a mobile multispectral imaging platform, PhenoField (PF) mounted on a jib crane for precise field phenotyping in wheat. % vegetation coverage and NDVI were correlated. Sharma *et al.* (2015) performed high-throughput phenotyping of cotton crop using a ground-based platform mounted on a research sprayer. Measurements of ground cover fraction (GCF) and NDVI were useful in determining growth and yield.

The disadvantage with vehicle operated platform is that they are difficult to operate in the crop at later stages even crop height is more. Recently a vehicle based platform with high clearance was reported. Murray *et al.* (2016) made self-propelled ground vehicles with adjustable heights for high clearance (over three meters of clearance) phenotyping in mature corn and sorghum without damage. It has sensors for RGB image capture, plant height estimation, vegetation indices, canopy temperature and PAR. These vehicles will be useful for monitoring growth in taller corn and sorghum plants that could be damaged by a tractor passing over them.

2.3.3. Unmanned Aerial Vehicles based systems

Unmanned aerial vehicles (UAV) equipped with camera and sensors can cover a large area in less time. Chapman *et al.* (2014) developed Phenocopter: a robotic helicopter for high-throughput field-based phenotyping over 0.5 to 3 ha experimental fields. Images were taken by three cameras - a normal camera, a camera with red-edge transmitting filter and a thermal (far-infrared) camera. The UAV could estimate variation in ground cover in sorghum (early season) and three-dimensional measures of crop lodging in wheat (late season). Bendig *et al.* (2014) provided method for estimating biomass of barley using crop surface models (CSMs) derived from UAV-based RGB imaging. They used multi-rotor MK-Oktokopter for taking RGB imagery with a digital camera from 50 m above. A high correlation was found between plant height from CSMs and fresh biomass (R^2 = 0.81) and dry biomass (R^2 = 0.82). Bendig *et al.* (2015) combined UAV-based plant height and vegetation indices for biomass monitoring in barley. UAV captured images at 2 frames per second (fps) at 50 m above ground level (AGL). Robust estimate for biomass were obtained from the plant height models (R^2 = 0.80–0.82). Liebisch *et al.* (2015) conducted aerial phenotyping of maize traits with a mobile multi-sensor approach using a Zeppelin NT aircraft as an experimental sensor platform. Measurements of canopy cover (CC) and its NDVI value and thermal images were done. Remotely sensed CC correlated well with plant density and early vigour. Sugiura *et al.* (2016) studied phenotyping system for potato late blight resistance using RGB imagery from an unmanned aerial vehicle (UAV) under field conditions. Area under the disease progress curves (AUDPCs) calculated from the time series of images was measured. They observed good correlation with biomass (R^2 = 0.73). Liebisch *et al.* (2016) reported a platform - Flourish for a robotic

approach for automation in crop management. The Flourish project - combined the aerial survey from small autonomous Unmanned Aerial Vehicle (UAV) with a multi-purpose Unmanned Ground Vehicle (UGV). RGB data using the excess green index and NDVI were used to estimate Crop canopy cover. Rasmussen *et al*. (2016) measured vegetation indices derived from cameras mounted on UAVs in winter barley and spring wheat. Excess green index (ExG) and Normalized green-red difference index (NGRDI) were closely correlated to biomass.

2.4. Ground cover and leaf area index estimation from images

The primary function of leaves is radiation interception and photosynthesis. This need of plant is achieved by an increase in leaf area. The growth of canopy is mostly visible due to the increase in numbers and expansion of leaves. The leaves then tend to cover the nearby space and the ground is shaded. The proportion of shaded ground is called ground cover. The canopy growth can be quantified in terms of increase in leaf area per unit land area called leaf area index (Watson 1947). With the increase in leaf area there is increase in radiation interception and crop growth. The radiation interception follows Lambert Beer's law (Monsi and Saeki 1953). Maximizing the interception of solar radiation by the canopy is an important component of biomass production and it is achieved by increase in leaf area as well as leaf architecture (Gardner *et al* 1985). Therefore estimates of leaf area index are important and are associated with the biomass production.

The direct measures of leaf area estimation are is destructive sampling. It is undesirable for estimation of large population of crop or canopy size such as forest trees. Therefore indirect measures have been used (Welles and Norman 1991). Jonckheere *et al*. (2004) have reviewed the methods for in situ leaf area index determination. The indirect methods include - inclined point quadrat (Wilson 1960, 63), allometric techniques especially for forests e.g. relation between sapwood area and leaf area (Gower and Norman 1991), stem basal area and leaf area (Bartelink 1997), diameter at breast height and leaf area (Le Dantec *et al* 2000) and optical non contact methods based on gap fraction analysis. Weiss (2004) has also reviewed the theoretical aspects of modeling the gap fraction and the leaf distribution profile. Therefore, indirect approaches related to radiation interception and its passage

through the canopy is useful for estimation of canopy growth (Welles 1990, Andrieu and Baret 1993, Welles and Cohen 1996).

One of the important and most widely used methods of estimating canopy growth is estimation of gap fraction. The gap fraction of a canopy is the fraction of view that is unobstructed by canopy in any particular direction (Welles and Cohen 1996). Alternatively, the gap fraction of a canopy is the fraction of view in some direction from beneath a canopy that is not blocked by foliage. Canopy gap fraction (P_0) is related to total plant area index (Lt) in accordance with the Beer-Lambert law (Nilson, 1971), $Po(\theta) = \exp((-G(\theta)\Omega(\theta)L_t)/\cos(\theta))$. Warren Wilson (1960) made an analytical study on inclined point quadrats and found that when the quadrat inclination was 32.5^o the variation in the relative frequency resulting from differences in foliage angle was lowest. Thus, the quadrat inclined at 32.5 degree resulted in greatly reduced errors. Wilson (1963) showed that at zenith angle 57.5°, the gap fraction is almost independent of leaf inclination simplifying the LAI retrieval process. This has therefore become the basis for deriving plant area index from the 57.5◦ gap fraction (Weiss *et al.*, 2004). At zenith angle 57.5°, the gap fraction approaches 0.5, and effective LAI can be estimated as $LAI = -\ln T(57.5^o).\cos(57.5^o)/0.5$, or, $L = \ln(Po(57.5^o))/0.931$.

There have been many studies to estimate the plant area index from gap fraction measurements at a particular view angle or with hemispherical views. Some of the studies are as follows - Gardingen *et al.* (1999) made LAI estimates from clumped canopies using hemispherical view images. The estimates of LAI could be improved by segmented analysis compared to the conventional method. Garrigues *et al.* (2008) made comparative analysis of LAI retrieval from different methods (viz. LAI 2000, AccuPAR and hemispherical photography. They found that the effective Plant Area Index retrived from downward pointing digital hemispherical photographs was better than the optical instruments LAI 2000 and AccuPAR for short canopy. They concluded that the digital hemispherical photography is more robust in terms of sensitivity to illumination conditions, spatial sampling and ability to capture gap fraction from short canopy. Demarez *et al.* (2008) estimated leaf area of wheat, sunflower and maize canopies with hemispherical photographs. LAI was computed with Poission law from measurements of unidirectional gap fraction. There was a

good correlation (r = 0.95) for the overall LAI estimates in these crops versus destructive LAI estimation. Liu and Pattey (2010) estimated the vertical gap fraction with the help of top of the canopy digital colour photography in maize, soybean and wheat canopies. They observed that the LAI estimates from photographs were comparable to LAI2000 estimates (R^2 = 0.83). Baret *et al*. (2010) made green area index estimates in wheat crop from downward looking digital photos taken at 57.5^o angle. There was a good agreement between the LAI estimates between the images and LAI2000 Canopy Analyzer estimates. Liu *et al.* (2013) made LAI measurements using the quantification of gap fraction at nadir or at 57.5^o view angle. They found a good association between destructive and observed LAI estimates (R^2 > 0.83). Confalonieri *et al*. (2013) made an app for leaf area index estimation using a smartphone based on the estimation of gap fraction at 57.5^o. The performance was similar to LAI2000 although less precise.

Another approach for canopy growth estimation is to measure the proportion of ground covered by the crop or the percentage of soil surface covered by plant foliage from digital images. Digital image analysis of photographs helps in quantitatively measuring the green vegetation from the total ground area. This parameter is also called digital ground cover (DGC). High early DGC helps in better interception of incident radiation, increases soil shading, decreases soil evaporation, increases water use efficiency, reduces weeds and soil erosion. Mullan and Reynolds (2010) and Mullan *et al.* (2012) described estimation of DGC in wheat using color digital camera with the help of Photoshop software. This method is most efficient till the ground cover is not complete. Campillo *et al*. (2010) estimated the LAI in vegetable crops by using digital images. The percentage of ground cover (PGC) and measured LAI were highly correlated (R^2 > 0.88). Kirk *et al.* (2009) provided a method for LAI estimation based on the red-green images taken from above the crop canopy in cereal crops. The method was found useful for initial as well as later stages of crops whereas the Canopy Analyzer is not useful for initial crop growth. Under controlled conditions the progress in leaf area development was studied by van der Heijden *et al*. (2012) and Horgan *et al*. (2015). They measured the progress of leaf area development over a height of 3 m in tall pepper (*Capsicum annuum* L.) plants in the greenhouse. The device was equipped with several cameras to capture images

upwards at intervals. With this approach they could find an earlier identified QTL related to leaf area growth.

Chapter 3

MATERIALS AND METHODS

The present study was conducted in the Division of Plant Physiology, Indian Agricultural Research Institute (IARI), New Delhi, during 2015-2016. The crops were sown in the Plant Physiology Field no. Genetics G, IARI, New Delhi.

3.1. Plant material and field experiment layout

Six genotypes of wheat namely- HD2967, Pusa Gold, HD2932, WH542, C306 and Kalyansona differing in their growth habit (e.g. tall, dwarf, early, late types) were sown in field. Sowing was done on 24th November and seed rate of 100 Kg/ha was used. Field experiment layout was in RBD with 3 replications (18 plots). Each plot (2.5 m x 7 m size) consisted of one genotypes sown in 10 rows at spacing of 25 cm (**Fig.1**). Plant population was maintained @ 17 plants per 30 cm row length based on the seed weight and spacing considerations. The 30 cm row length containing 17 plants was marked with aluminum labels for identification during sampling. The fertilizers were applied @ 120 Kg N/ha, 60 kg P_2O_5/ha, 60 K_2O/ha as per recommended practices. Five irrigations were applied during entire crop period.

3.2. Dry Weight Sampling and Image Acquisition

All field observations (growth parameters, biochemical) were taken in three replicates. Samples were taken from 30 cm row length of crops consisting 17 plants. Destructive sampling for leaf area and dry weight measurement was done at 9 to 14 days intervals starting from 22 DAS to 96 DAS (**Plate 1 and 2**). Dry weight sampling and processing was done within 24 hours of imaging. Collected shoot and leaves were dried in hot air oven at 70^{o}C for 4 hours and then at 60^{o}C till constant weight were reached and then dry weight recorded.

Before dry matter sampling, images of crop samples were taken. Images of side view of canopy (**Plate 3**) were taken from the space between the rows. The concept of side view in relation to biomass estimation has been provided earlier by Takenberg (2007), Golzarian (2011) and also reviewed by Fiorani and Schurr (2013). Side view was taken using a DSLR camera (Nikon D5200) attached to a customized

imaging set-up. The description of the imaging system is not presented here due to the IPR application issues. Top view images (**Fig.2**) were taken as described by Mullan and Reynolds (2010) and Mullan and Garcia (2012).

3.3. Leaf Area measurement

For leaf area measurement the samples were taken from 30 cm row length of crops consisting 17 plants. Leaves were detached and the leaf area was measured by using leaf area meter (LI-3100).

3.4. Leaf Chlorophyll content

Chlorophyll content was estimated at 22, 32, 42, 53, 63, 73, 82 and 96 days after sowing (DAS). Chlorophyll extraction was done as per the method described by Hiscox and Israelstam (1979). 50 mg fresh leaf samples were added to the test tubes containing 10 ml DMSO with 3 replications per sample. Tubes were kept in dark for 4 hours at 65 ^{0}C. After then the samples were taken out from dark and cooled at room temperature and the absorbance of known volume of solution containing known quantity of leaf tissue at five respective wavelengths (480, 645, 649, 663 and 665 nm) were taken and using DMSO as blank. Chlorophyll a, chlorophyll b, total chlorophyll and carotenoids content were estimated using the formula given by Wellburn, (1994) and expressed as mg g^{-1} fresh weight.

Chlorophyll ‘a’ (C_a)= $(12.19 \times A_{665} - 3.45 \times A_{649}) \times V/W \times 1000$

Chlorophyll ‘b’(C_b)= $(21.99 \times A_{649} - 5.32 \times A_{665}) \times V/W \times 1000$

Total Chlorophyll= $C_a + C_b$

Total carotenoids= $(1000 \times A_{480} - 2.14 \times C_a - 70.16 \times C_b) \times V/220 \times W \times 1000$

Where, A_{665} = Absorbance values at 665 nm

A_{649} = Absorbance values at 649 nm

A_{480} = Absorbance values at 480 nm

W = Weight of the sample (g);

V = Volume of solvent (ml)

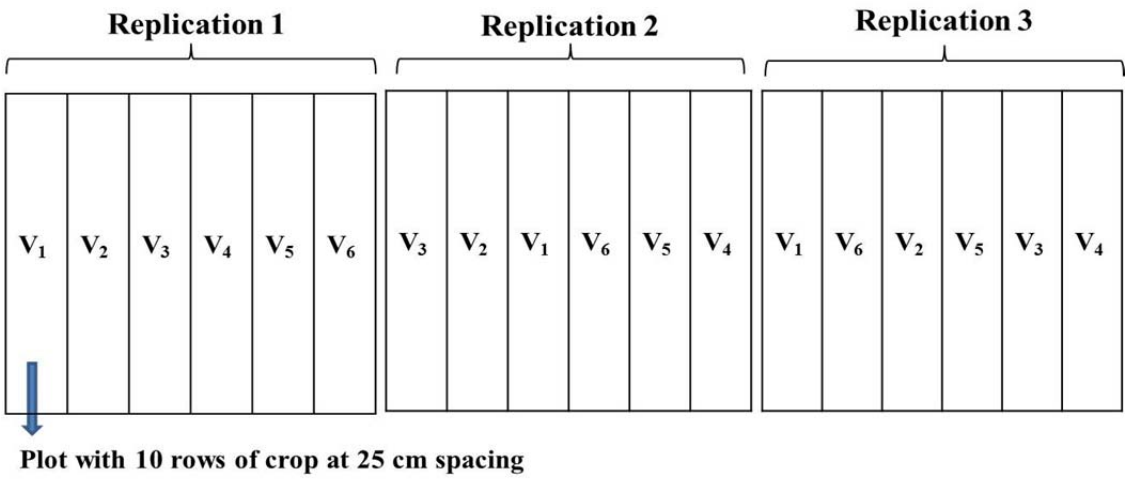

Fig.1: Crop experiment layout in field.

Note: 1. Design - Randomized Block Design with 3 replications.

2. Treatments - six wheat genotypes

V1 – HD2967	**V3 – HD2932**	**V5 – C306**
V2 – Pusa Gold	**V4 – WH542**	**V6 – Kalyansona**

.

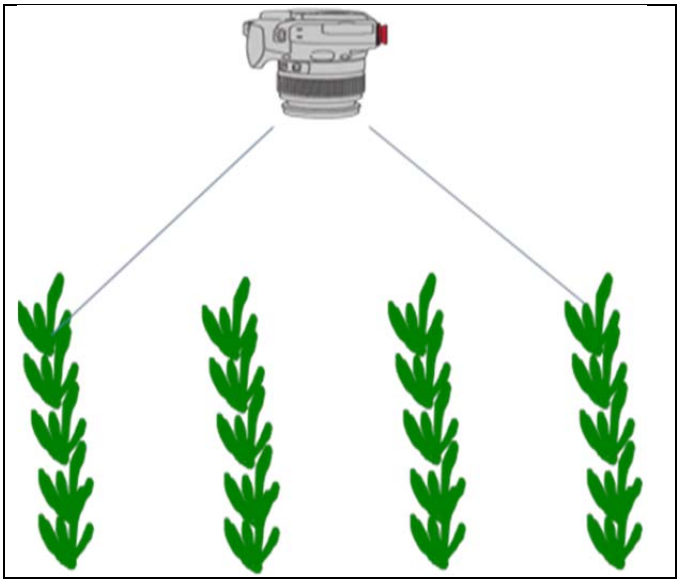

Fig.2: Diagram to capture the top view image of wheat crop rows.

Plate.1: Wheat crop field view at 30 DAS.

Plate.2: Wheat crop field view at 95 DAS.

Plate.1 & 2: Experimental set up of six wheat genotypes in the field. (Sowing date: 24 Nov., 2015).

Plate.3: Side view image of wheat crop row (30 cm) at 33 DAS.

Plate.4: Bottom to top image of canopy at 57^{o} angle.

3.5. Calculation of growth parameters

Calculation of different growth parameters of six genotypes of wheat was done according to the following methods -

Growth parameters (unit)	Formula	Reference
Average growth rate ($g\ day^{-1}$)	$AGR = (W_2 - W_1)/(T_2 - T_1)$	Evans (1972)
Relative growth rate ($mg\ g^{-1}\ day^{-1}$)	$RGR = (\ln W_2 - \ln W_1)/(T_2 - T_1)$	Blackman (1919)
Crop growth rate ($g\ m^{-2}\ day^{-1}$)	$CGR = 1/G_A \times (W_2 - W_1)/(T_2 - T_1)$	Watson (1952)
Leaf area index (unit less)	$LAI = L_A/G_A$	Watson (1947)
Leaf area ratio ($cm^2\ g^{-1}$)	$LAR = L_A/W$	Evans (1972)

Where, W_1= Dry weight at time T_1

W_2 = Dry weight at T_2

G_A= Ground area occupied by canopy

L_A= Leaf area

3.6. Images processing

3.6.1. Measurement of Projected Area from side view of crops

Side view images were processed by 'ImageJ' software. It is an open source software developed by NIH, USA. The color image was converted to grayscale (8 bit). The background subtraction was done depending on the type of background. Image thresholding helped in the identification of crop projected area in comparison to the background (Zack, 1977). After that, image analysis was done to get the % area of image occupied by plants. From this actual projected area (cm^2) was estimated based on the reference frame.

3.6.2. Digital ground cover (%) - top view of crops

Top view images (**Fig.2**) were taken as described by Mullan and Reynolds (2010) and Mullan and Garcia (2012). The reference frame was set to 30 cm row length for the present work. Processing of digital ground cover images was done using 'Adobe Photoshop CS5' software. The analysis includes - opening the image in Photoshop, picking the green pixels from the plant canopy and transforming the image into black and white with white indicating canopy and black indicating background. Then, the black and white image is used to estimate the % canopy area (i.e. the proportion of white pixels) as per Mullan and Reynolds (2010). The percentage ground cover (%GC) for the photograph is calculated using the equation-

$$\%GC = (\text{Mean Grey Value}/ 255) \times 100$$

3.7. Estimation of biomass and growth based on projected area

The biomass is positively related with the image projected area (Leister *et al.* 1999, Tackenberg 2007); therefore biomass was indirectly estimated from the side view image projected area. Also, Greider *et. al.* (2015) estimated RGR in wheat non-destructively under field conditions using NDVI canopy cover images. So the crop growth parameters viz. AGR, RGR and CGR can be calculated using image based projected area by following formulas:

Formula	Unit
$AGR = (PA_2\text{-}PA_1) / (T_2 - T_1)$	cm^2 PA day^{-1}
$RGR = [\ln(PA_2) - \ln(PA_1)] / (T_2 - T_1)$	cm^2 PA cm^{-2} PA day^{-1}
$CGR = 1/GA \times (PA_2 - PA_1) / (T_2 - T_1)$	cm^2 PA cm^{-2} GA day^{-1}

Where, PA_2 = Projected area at time T_2

PA_1= Projected area at time T_1 and GA = Ground area occupied by canopy

3.6.3. Bottom to top image of canopy at 57^o angle

In another experiment, images of bottom to top view of canopy (**Plate 4**) were taken in 47 wheat genotypes at 63 DAS stage by a mobile phone at 57^o angle from zenith as per Weiss *et al.* (2004). Foliage area projected to the 57.5^o direction is approximately equal to 0.5 regardless of leaf angle distribution. This is the basis for deriving plant

area index from the 57.5^{o} gap fraction (Weiss *et al.*, 2004). The same samples were cut and observation on total leaf area and dry weight were taken. LAI was also measured using plant canopy analyzer instrument (LAI-2000).

Processing of images was done by ImageJ software to estimate gap fraction or the visible sky area. The gap fraction is the fraction of view in some direction from beneath a canopy that is not blocked by foliage (Welles and Cohen 1996). The effective LAI can be derived with the following equation (Weiss *et al.*, 2004):

$$\mathbf{LAI} = - \ln P_o (57.5^{o}) / 0.931$$

Where, LAI = Leaf area index

P_o= canopy gap fraction

3.8. Statistical analysis

All statistical analysis was performed for RBD design as per the procedures described by Gomez and Gomez (1984). In one instance a missing replication was analyzed as per Gomez and Gomez (1984). The statistical parameters such as CD, SEM, CV were computed by using OPSTAT, open source statistical software developed by O.P. Sheoran Programmer, Computer Section, CCS HAU, Hisar Statistical were followed. Graphs were prepared from the mean value with $\pm$SEm values.

Chapter 4

RESULTS

4.1. Dry matter production, partitioning and its relationship with side view image based projected area.

4.1.1. Above-ground crop dry weight

The progress of above-ground plant dry weight (g) increase at different DAS from (30 cm row length of crop) in six wheat genotypes is shown in (**Fig.3**) and each mean value in the graph is provided with ±SEm. The mean above-ground crop dry weight was found highest at 96 DAS stage (**Table1**). The highest above-ground plant dry weight was observed in wheat genotype C306 at 96 DAS stage. This genotype was significantly different over the genotypes HD2967, Pusa Gold, HD2932, WH542 and Kalyansona. There was significant difference between the genotypes for plant dry weight at 42, 63, 73, 82 and 96 DAS. But, there was no significant difference between the genotypes for plant dry weight at 22, 32 and 53 DAS.

4.1.2. Leaf dry weight

The leaf dry weight (g) at different DAS from 30 cm row length of crop in six wheat genotypes is shown in (**Fig.4**). The mean leaf dry weight was found highest at 82 DAS stage. The highest leaf dry weight was observed in wheat genotype C306 at 73 DAS stage. This genotype was significantly different over the genotypes HD2967, Pusa Gold, HD2932, WH542 and Kalyansona. There was significant difference between the genotypes for leaf dry weight at 32, 42, 73, 82 and 96 DAS (**Table2**). But, there was no significant difference between the genotypes for leaf dry weight at 22 and 53 DAS.

4.1.3. Progress of dry matter production, image based projected area and dry matter partitioning with time in wheat genotypes.

The data on the dry matter production and image based projected area is given in **Table 1 and 3** respectively.

4.1.3.1. Wheat genotype HD2967

The dry matter production and image based projected area followed similar pattern from 22 DAS to 96 DAS in wheat variety HD2967 as shown in (**Fig.5**). Dry matter partitioning between leaves and shoot in HD2967 is given in (**Fig.6**). Leaf dry matter was highest at 82 DAS and consisted of 40.3% of total plant above-ground dry weight; whereas the shoots dry weight (including ear) was 59.7%. At 96 DAS the leaf dry matter decreased and it was 25.5% of total dry matter of plant whereas the shoot dry matter increased to 74.5%.

4.1.3.2. Wheat genotype Pusa Gold

Progress of dry matter production and image based projected area followed similar pattern of growth in Pusa Gold genotype from 22 DAS to 96 DAS as given in (**Fig.7**). Dry matter partitioning between leaves and shoot in Pusa Gold is given in (**Fig.8**). Leaf dry matter was highest in Pusa Gold genotype at 73 DAS that was 23.6% of total plant above-ground dry weight at same time shoot dry weight (including ear) was 76.4%. At 96 DAS leaf dry matter decreased to 11.4% of total dry matter of plant and the shoot dry matter increased to 88.6%.

4.1.3.3. Wheat genotype HD2932

Progress of dry matter production and image based projected area followed similar pattern of growth in HD2932 genotype from 22 DAS to 96 DAS as given in (**Fig.9**). Dry matter partitioning between leaves and shoot in HD2932 is given in (**Fig.10**). Leaf dry matter was highest in HD2932 genotype at 63 DAS that was 40% of total plant above-ground dry weight at same time shoot dry weight (including ear) was 60%. At 96 DAS, leaf dry matter decreased to 12.7% of total dry matter and the shoot dry matter increased to 87.3%.

4.1.3.4. Wheat genotype WH542

Progress of dry matter production and image based projected area followed similar pattern of growth in WH542 genotype from 22 DAS to 96 DAS as given in (**Fig.11**). Dry matter partitioning between leaves and shoot in WH542 is given in (**Fig.12**). Leaf dry matter was highest in WH542 genotype at 82 DAS that was 35.1% of total plant above-ground dry weight at same time shoot dry weight (including ear) was 64.9%.

Table 1: Above-ground crop dry weight (g) at different DAS from 30 cm row length of crop in six wheat genotypes

Wheat genotypes	Day after sowing							
	22	32	42	53	63	73	82	96
HD2967	1.149	2.900	7.124	12.557	18.733	24.200	36.987	54.120
Pusa Gold	1.025	3.468	6.887	14.083	24.220	44.427	45.333	62.467
HD2932	1.046	2.761	9.497	15.020	31.090	30.187	41.930	66.790
WH542	0.837	2.701	4.134	11.297	14.917	32.970	42.497	59.133
C306	1.009	3.162	9.005	21.773	35.281	65.832	78.877	102.060
Kalyansona	0.784	1.956	4.728	12.140	23.583	37.533	50.633	63.740
Mean	0.975	2.825	6.896	14.478	24.637	39.192	49.376	68.052
CD at 5%	N/A	N/A	1.906	N/A	6.773	19.214	12.933	20.627
CV (%)	19.311	18.201	14.997	28.742	14.918	26.604	14.214	16.449

Table 2: Leaf dry weight (g) at different DAS from 30 cm row length of crop in six wheat genotypes

Wheat genotypes	Day after sowing						
	22	32	42	53	73	82	96
HD2967	0.820	1.941	4.454	7.553	12.697	14.923	11.020
Pusa Gold	0.763	2.359	4.278	7.160	10.487	7.687	7.183
HD2932	0.777	1.886	5.822	7.567	8.780	10.353	8.487
WH542	0.598	1.809	2.735	6.663	14.707	14.953	10.850
C306	0.800	2.234	6.170	12.633	23.046	21.656	14.500
Kalyansona	0.614	1.338	2.988	7.177	15.320	15.873	10.477
Mean	0.729	1.928	4.408	8.126	14.173	14.241	10.419
CD at 5%	N/A	0.595	1.307	N/A	6.214	4.865	3.598
CV (%)	17.104	16.742	16.086	27.843	23.794	18.538	18.741

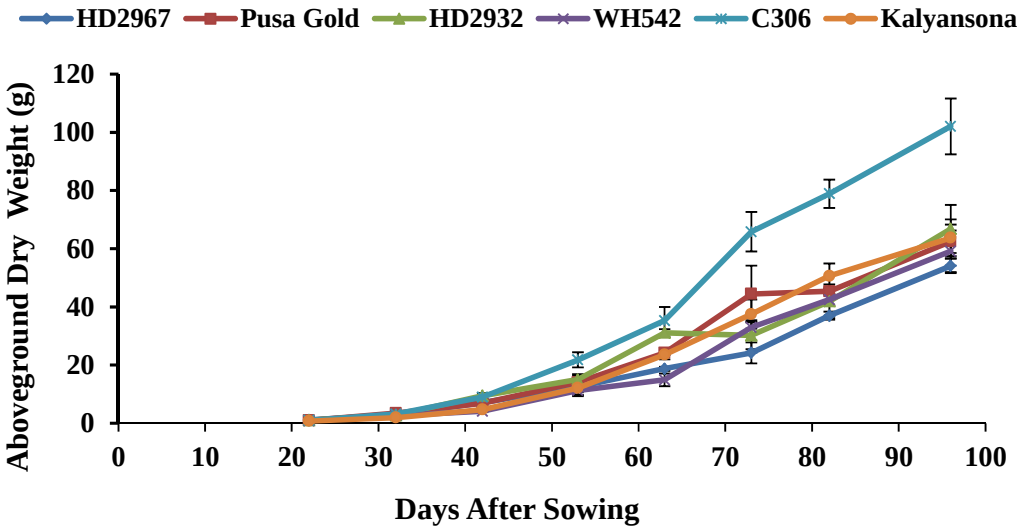

Fig.3: Above-ground crop dry weight (g) at different DAS from 30 cm row length in six wheat genotypes

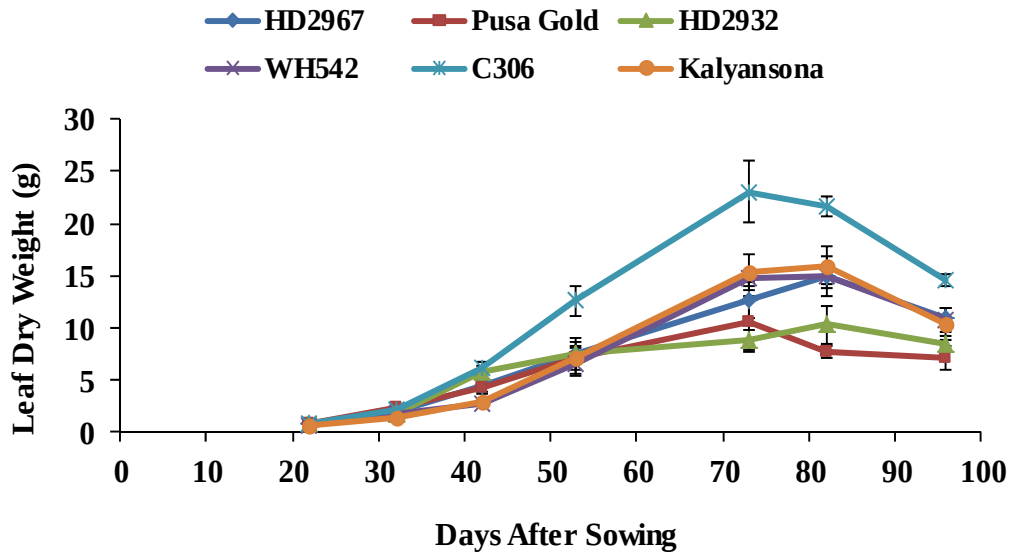

Fig.4: Leaf dry weight (g) at different DAS from 30 cm row length in six wheat genotypes

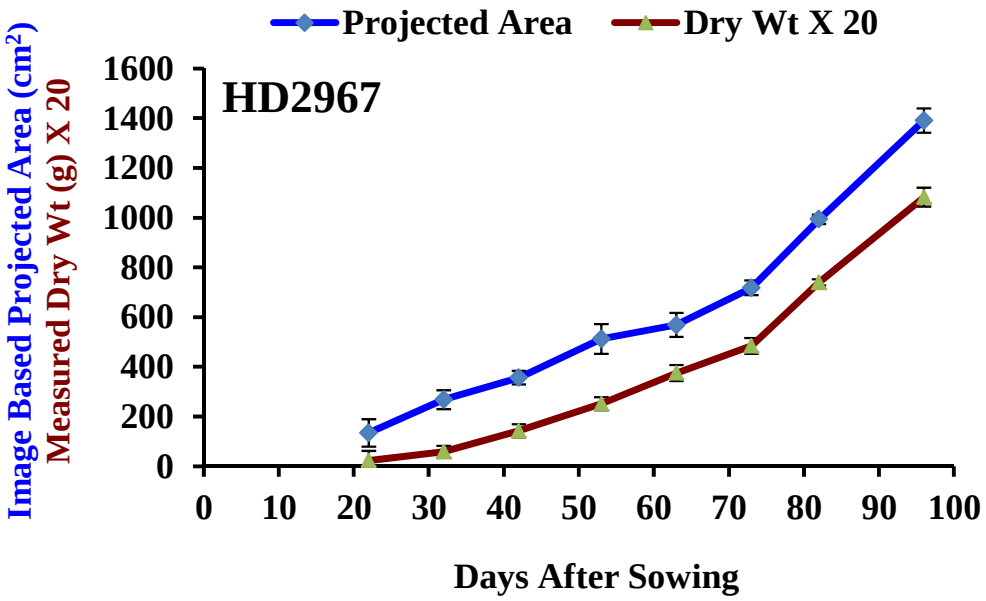

Fig.5: Progress of dry matter production and image based projected area at different DAS in HD2967 genotype

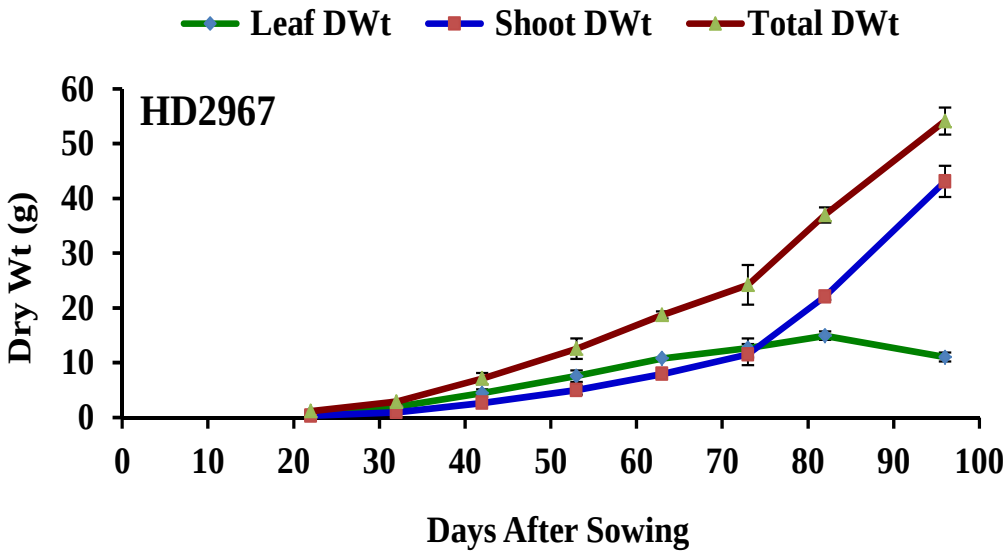

Fig.6: Progress of dry matter partitioning at different DAS in HD2967 genotype

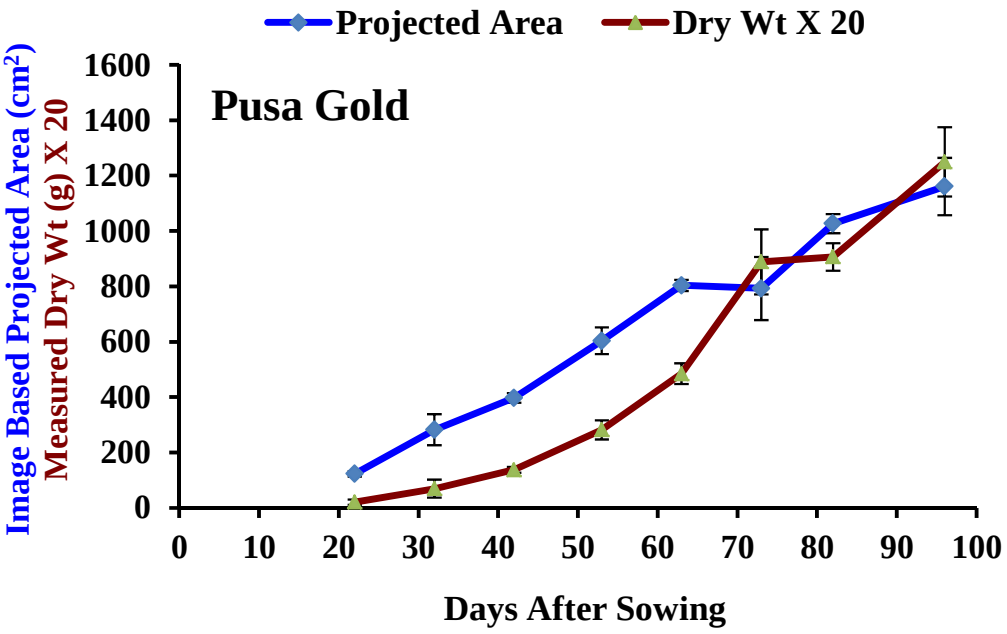

Fig.7: Progress of dry matter production and image based projected area at different DAS in Pusa Gold genotype

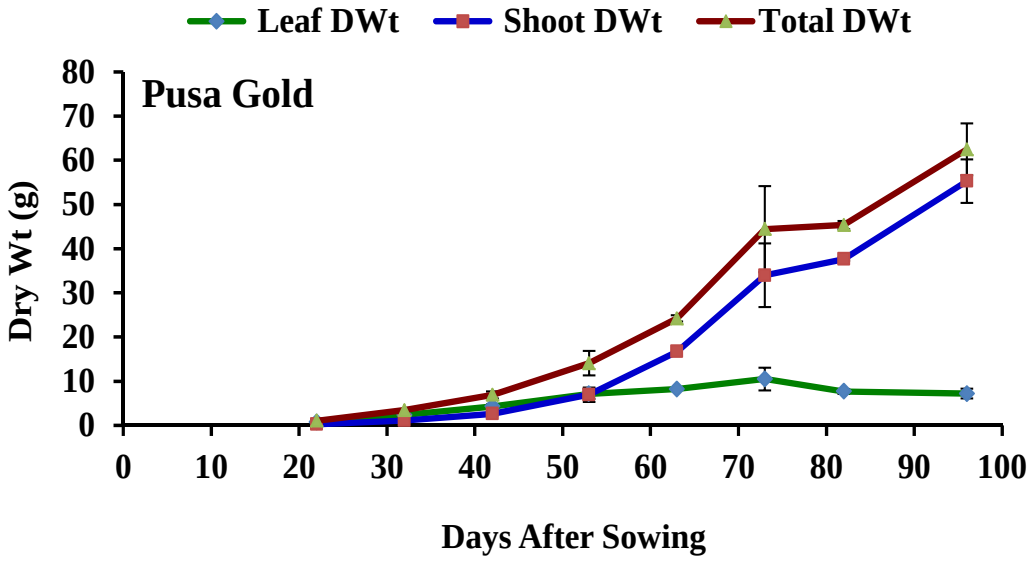

Fig.8: Progress of dry matter partitioning at different DAS in Pusa Gold genotype

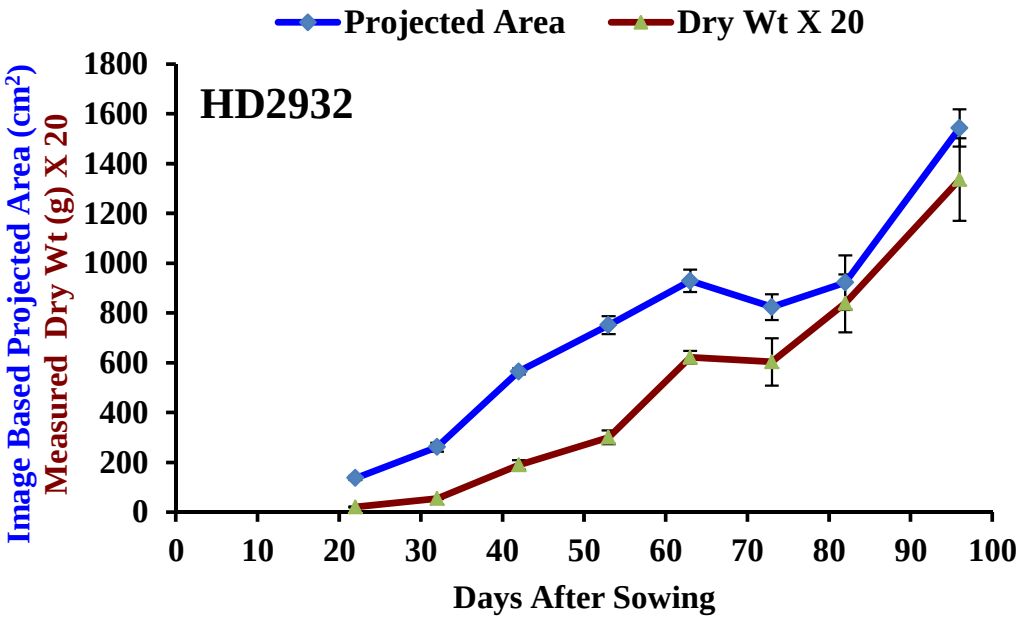

Fig.9: Progress of dry matter production and image based projected area at different DAS in HD2932 genotype

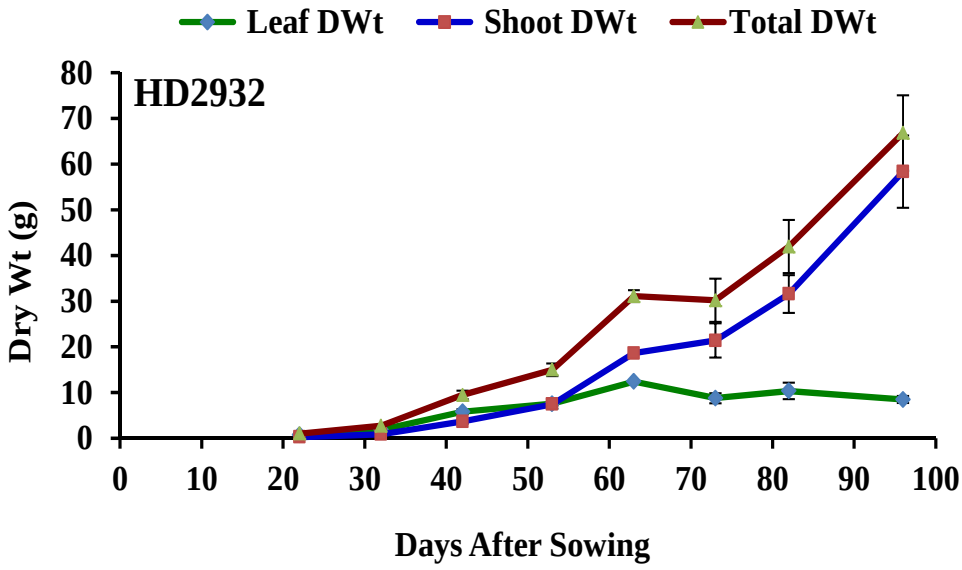

Fig.10: Progress of dry matter partitioning at different DAS in HD2932 genotype

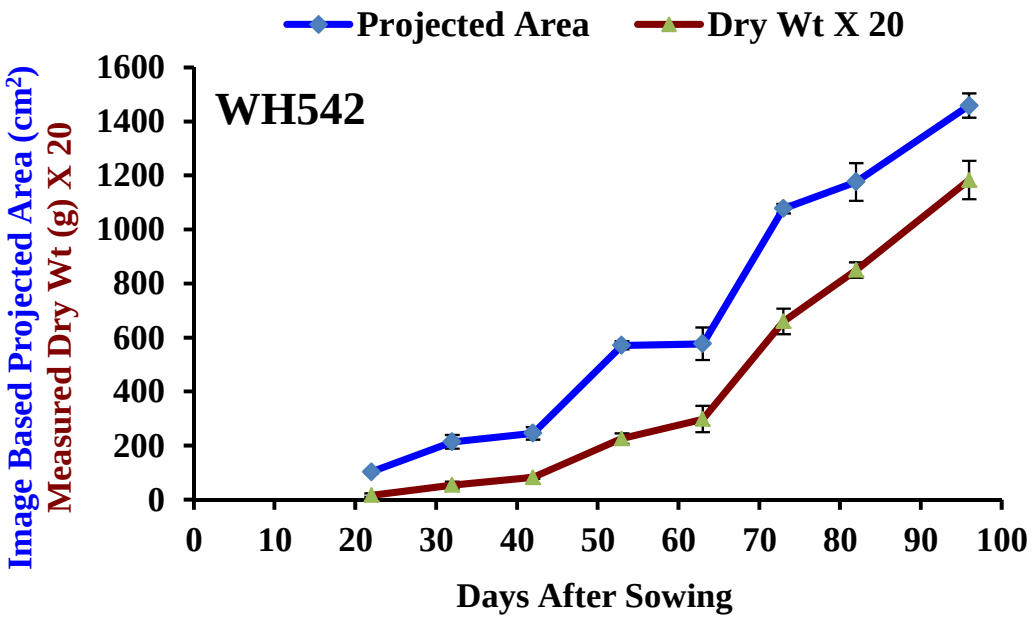

Fig.11: Progress of dry matter production and image based projected area at different DAS in WH542 genotype

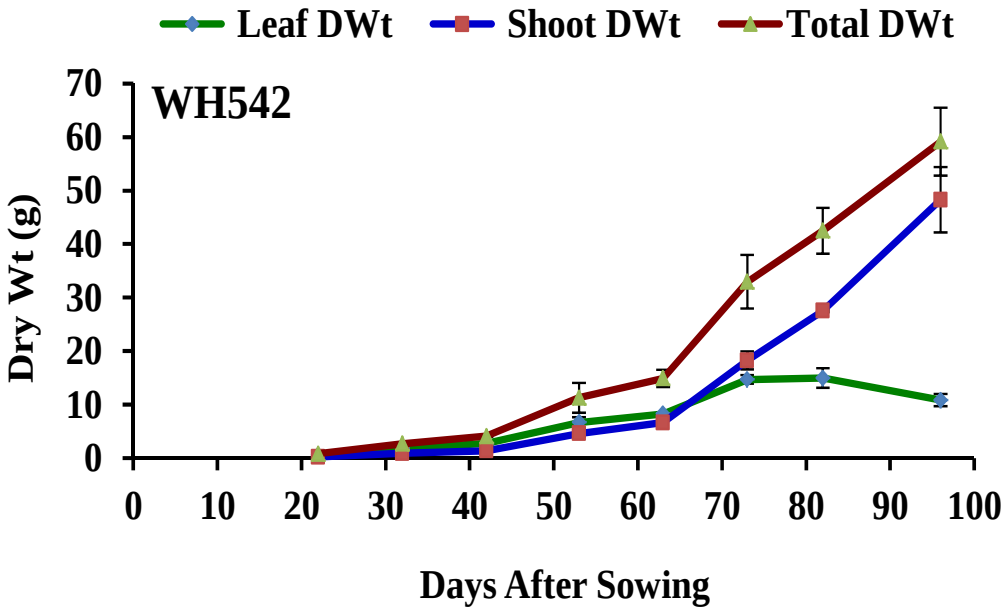

Fig.12: Progress of dry matter partitioning at different DAS in WH542 genotype

Table 3: Projected area of image (cm^2) at different DAS from 30 cm row length of crop in six wheat genotypes

Wheat genotypes	Day after sowing							
	22	32	42	53	63	73	82	96
HD2967	134.096	267.809	356.199	512.021	568.687	717.415	993.534	1390.682
Pusa Gold	122.889	282.128	397.564	603.480	803.323	792.703	1027.009	1160.785
HD2932	137.474	261.622	564.560	751.198	929.054	823.561	921.793	1543.006
WH542	103.068	214.061	245.475	570.601	576.470	1077.388	1175.903	1458.564
C306	126.127	222.398	495.728	892.816	1031.649	1656.891	1813.528	2161.184
Kalyansona	104.948	166.868	321.699	570.580	815.089	1105.213	1135.996	1627.779
Mean	121.434	235.814	396.871	650.116	787.379	1028.862	1177.961	1557.000
CD at 5%	22.677	N/A	63.300	172.430	144.822	220.131	240.408	261.368
CV (%)	10.151	25.521	8.655	14.393	9.981	11.611	11.075	9.109

Table 4: LAR ($cm^2\ g^{-1}$) at different DAS from 30 cm row length of crop in six wheat genotypes

Wheat genotypes	Day after sowing						
	22	32	42	53	73	82	96
HD2967	131.642	117.149	119.863	108.657	94.610	63.249	31.924
Pusa Gold	138.634	125.843	122.516	94.059	41.579	25.011	18.554
HD2932	145.139	136.330	139.204	106.345	52.341	38.014	22.805
WH542	121.616	122.427	124.321	102.095	81.836	55.538	26.967
C306	148.976	125.490	130.657	124.178	70.303	44.470	24.153
Kalyansona	128.219	129.141	122.982	112.875	75.425	43.236	27.128
Mean	135.704	126.063	126.590	108.035	69.349	44.920	25.255
CD at 5%	15.590	6.993	8.198	12.035	9.023	5.339	6.383
CV (%)	6.214	3.013	3.514	6.044	7.055	6.431	13.582

At 96 DAS leaf dry matter decreased to 18.3% of total dry matter and the shoot dry matter increased to 81.7%.

4.1.3.5. Wheat genotype C306

Progress of dry matter production and image based projected area following similar pattern of growth in C306 genotype from 22 DAS to 96 DAS is given in (**Fig.13**). Dry matter partitioning between leaves and shoot in C306 is given in (**Fig.14**). Leaf dry matter highest in C306 genotype at 73 DAS that was 35% of total plant above-ground dry weight at same time shoot dry weight (including ear) was 65%. At 96 DAS leaf dry matter decreased and it was 14.2% of total dry matter of plant. At 96 DAS shoot dry matter increased and it was 85.8%.

4.1.3.6. Wheat genotype Kalyansona

Progress of dry matter production and image based projected area followed similar pattern of growth in Kalyansona genotype from 22 DAS to 96 DAS as given in (**Fig.15**). Dry matter partitioning between leaves and shoot in Kalyansona is given in (**Fig.16**). Leaf dry matter was highest in Kalyansona genotype at 82 DAS that was 31.3% of total plant above-ground dry weight at same time shoot dry weight (including ear) was 68.7%. At 96 DAS leaf dry matter decreased to 16.4% and the shoot dry matter increased to 85.6%.

4.1.4. Leaf area ratio

The LAR at different DAS from 30 cm row length of crop in six wheat genotypes in which LAR was found highest at 22 DAS stage (**Table4**). The highest LAR was observed in wheat genotype C306 at 22 DAS stage. This genotype was significantly different over the genotypes HD2967, WH542 and Kalyansona. There was significant difference between the genotypes for LAR at 22, 32, 42, 53, 73, 82 and 96 DAS.

4.1.5. Correlation between measured dry weight and image based projected area

The correlation between measured dry weight (**Table1**) and image based projected area (**Table3**) parameter is given in (**Fig.17a,b,c**). It shows a highly significant correlation (r = 0.972**) between these parameters. Also, linear relationship between these parameters has a high R^2 value (0.945, y = 0.047x - 9.35) which can be useful for prediction of biomass from image based projected area [**Fig.17(a)**]. Similarly nonlinear relationship between these has a high R^2 value (0.952, y = 0.0000069x2 +

0.034x - 5.508) [**Fig.17(b)**] and log-log relationship showed highly significant correlation (0.990**) with a high R^2 value (0.980, y = 1.6667x - 1.08) [**Fig.17(c)**].

4.1.6. Correlation between dry weight based RGR and projected area based RGR

The correlation between dry weight based RGR (measured by destructive sampling) and projected area based RGR parameter is given in (**Fig.18**). The RGR values were taken for the points satisfying the exponential growth. A highly significant correlation (r = 0.898**) between these parameters. Also, there is a linear relationship between these with a high R^2 value (0.807, y = 1.0512x + 0.0294) which can be useful for prediction of RGR from projected area based RGR.

4.1.7. Correlation between dry weight based AGR and projected area based AGR

The correlation between dry weight based AGR and projected area based AGR parameter is given in (**Fig.19**). It shows a highly significant correlation (r = 0.520**) between these parameters. Also, the linear relationship between these have a high R^2 value (0.271, y = 0.025x + 0.4176) which can be useful for prediction of AGR from projected area based AGR.

4.1.8. Correlation between dry weight based CGR and projected area based CGR

The correlation between dry weight based CGR and projected area based CGR parameter is given in (**Fig.20**). It shows a highly significant correlation (r = 0.520**) between these parameters. Also, there linear relationship between these have a high R^2 value (0.471, y = 0.4597x + 0.9606) which can be useful for prediction of CGR from projected area based CGR.

4.2. Canopy growth and its relation with digital ground cover

4.2.1. Correlation between measured CGR and measured LAI.

The correlation between measured CGR and measured LAI parameter is given in (**Fig.21**). It shows a highly significant correlation (r = 0.719**) between these parameters. Also, there linear relationship between these have a high R^2 value (0.517, y = 4.8468x + 2.702).

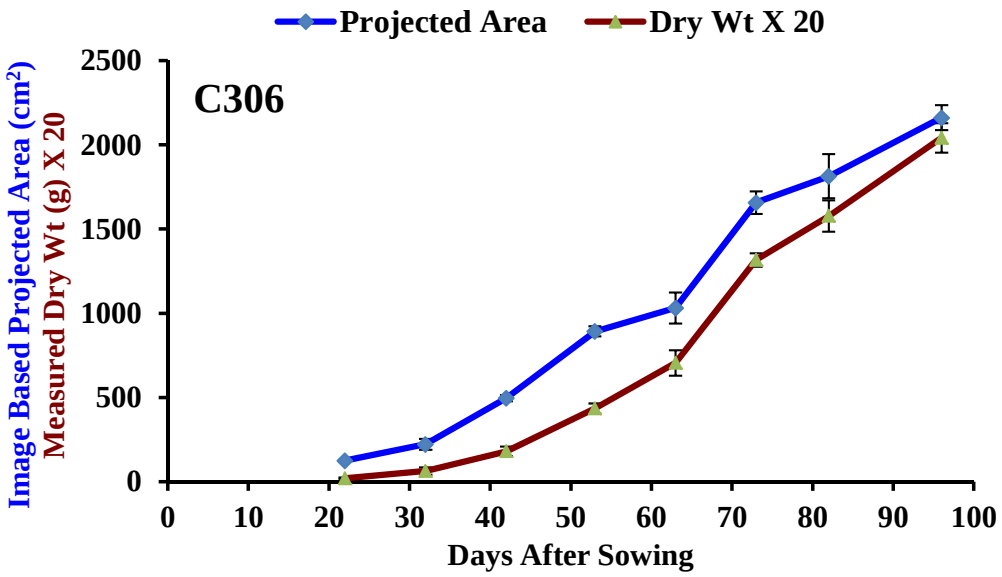

Fig.13: Progress of dry matter production and image based projected area at different DAS in C306 genotype

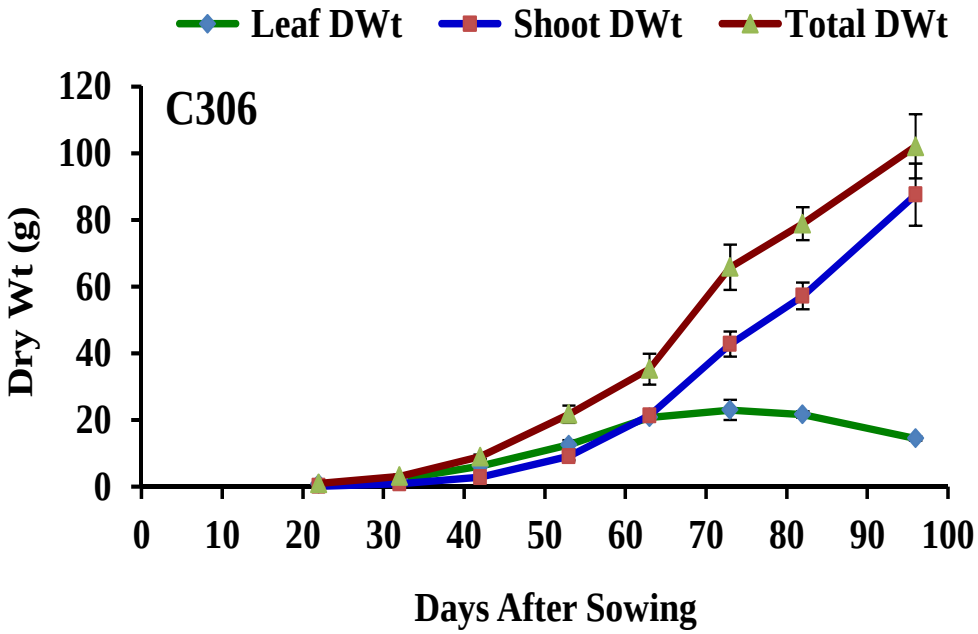

Fig.14: Progress of dry matter partitioning at different DAS in C306 genotype

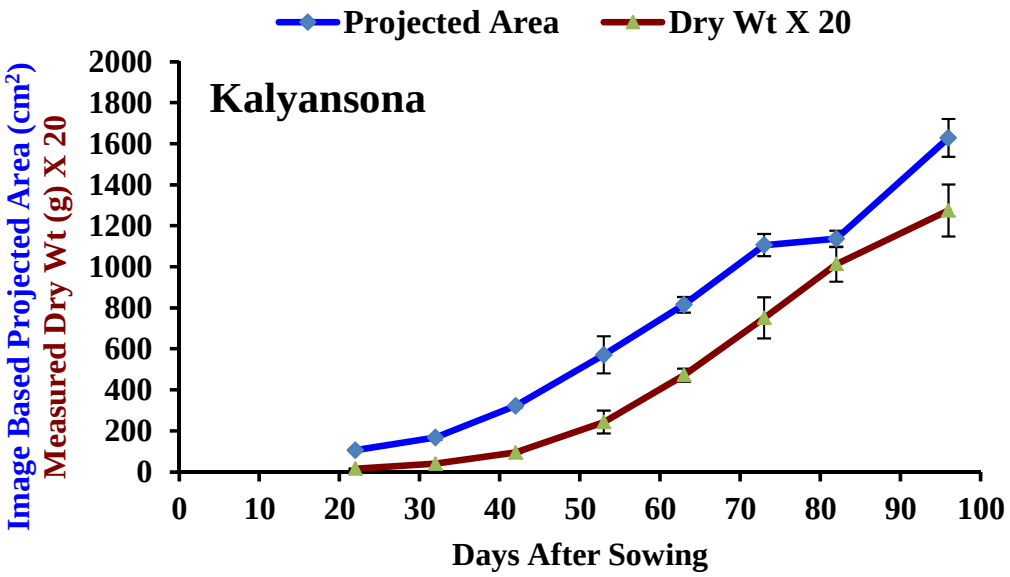

Fig.15: Progress of dry matter production and image based projected area at different DAS in Kalyansona genotype

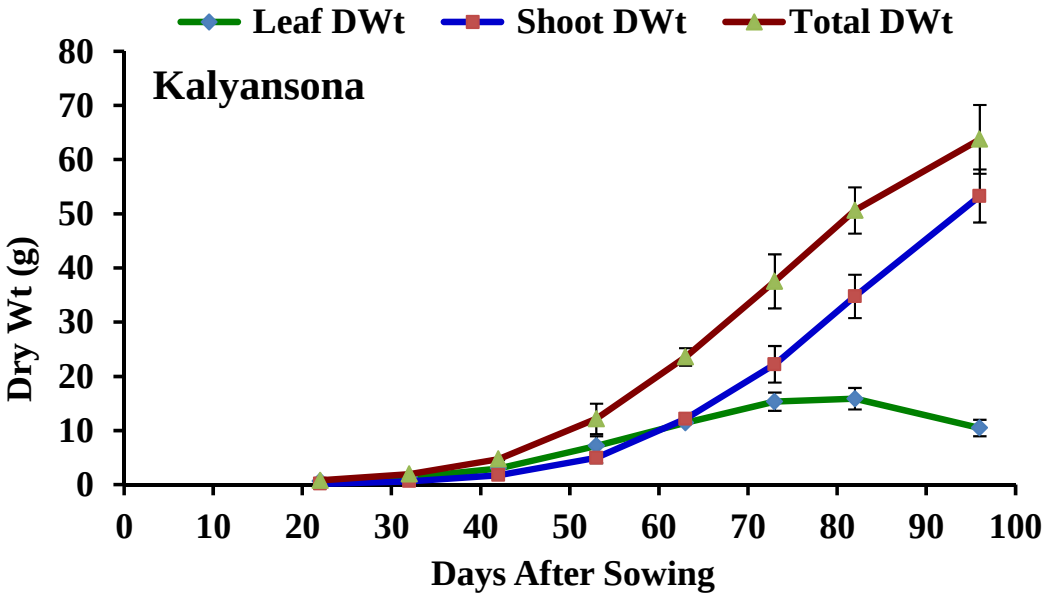

Fig.16: Progress of dry matter partitioning at different DAS in Kalyansona genotype

4.2.2. Leaf area index

The LAI at different DAS from 30 cm row length of crop in six wheat genotypes is shown in (**Fig.22**). The LAI was found highest at 73 DAS stage. The highest LAI was observed in wheat genotype C306 at 73 DAS stage. This genotype was significantly different over the genotypes HD2967, Pusa Gold, HD2932, WH542 and Kalyansona **(Table5**). There was significant difference between the genotypes for LAI at 22, 42, 53, 73, 82 and 96 DAS. But, there was no significant difference between the genotype for LAI at 32 DAS**.**

4.2.3. % Digital ground cover

The % digital ground cover at different DAS from 30 cm row length of crop in six wheat genotypes is shown in [**Fig.23(a)**]. The % digital ground cover was found highest at 53 DAS stage. The highest % digital ground cover was observed in wheat genotype C306 at 53 DAS stage. However, this genotype was not significantly different over the other genotypes (**Table 6**). There was significant difference between the genotypes for % digital ground cover at 42 DAS. But, there was no significant difference between the genotypes for % digital ground cover at 22, 32 and 53 DAS.

4.2.4. Correlation between measured leaf area and % digital ground cover

The correlation between measured leaf area and % digital ground cover parameter is given in [**Fig.23(b)**]. It shows a highly significant correlation (r = 0.919**) between these parameters. Also, there linear relationship between these have a high R^2 value (0.845, y = 32.737x - 319.65) which can be useful for prediction of leaf area % from digital ground cover.

4.2.5. Correlation between measured dry weight and % digital ground cover

The correlation between measured dry weight and % digital ground cover parameter is given in [**Fig.23(c)**]. It shows a highly significant correlation (r = 0.901**) between these parameters. Also, there linear relationship between these have a high R^2 value (0.812, y = 0.282x - 2.8249) which can be useful for prediction of dry weight from % digital ground cover.

4.3. Canopy growth from gap fraction analysis with mobile phone

4.3.1. Correlation between actual LAI and gap fraction based LAI

The correlation between actual LAI and projected area based LAI parameter is given in [**Fig.24(a)**]. It shows a high correlation (r = 0.725**) between these parameters. Also, there linear relationship between these have a high R^2 value (0.527, y = 1.7483x + 0.7945) which can be useful for prediction of actual LAI from projected area based LAI.

4.3.2. Correlation between LAI with canopy analyzer and gap fraction based LAI

The correlation between LAI with canopy analyzer and gap fraction based LAI parameter is given in [**Fig.24(b)**]. It shows a highly significant correlation (r = 0.736**) between these parameters. Also, there linear relationship between these have a high R^2 value (0.542, y = 0.7331x + 0.4531) which can be useful for prediction of LAI from projected area based LAI.

4.3.3. Correlation between LAI with canopy analyzer and actual LAI

The correlation between LAI measure with canopy analyzer and actual LAI parameter is given in [**Fig.24(c)**]. It shows a highly significant correlation (r = 0.757**) between these parameters. Also, there is a linear relationship between these with a high R^2 value (0.574, y = 0.3178x + 0.3978).

4.4. Leaf pigment estimation in wheat genotypes

4.4.1. Chlorophyll and carotenoid content on fresh weight basis

4.4.1.1. Total chlorophyll content

The total chlorophyll content at different DAS in six wheat genotypes is shown in (**Table7**). The total chlorophyll was found highest at 96 DAS stage. The highest total chlorophyll was observed in wheat genotype Pusa Gold at 96 DAS stage. This genotype was however not significantly different over the other genotypes. There was significant difference between the genotypes for total chlorophyll 73 DAS. But, there was no significant difference between the genotypes for total chlorophyll at 22, 32, 42, 53, 63, 82 and 96 DAS.

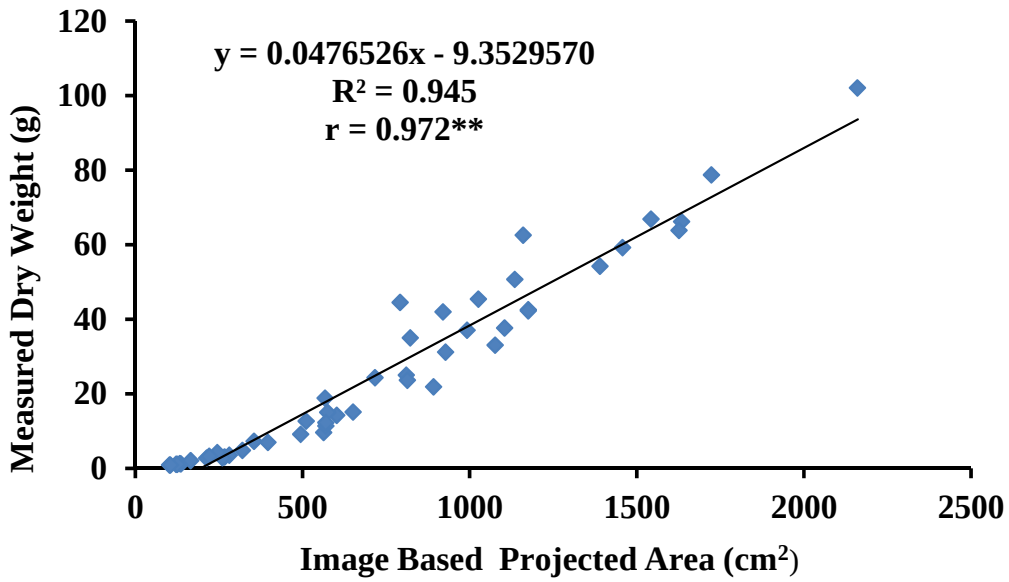

Fig.17 (a): Linear relationship between dry weights measured by destructive sampling and image based projected area

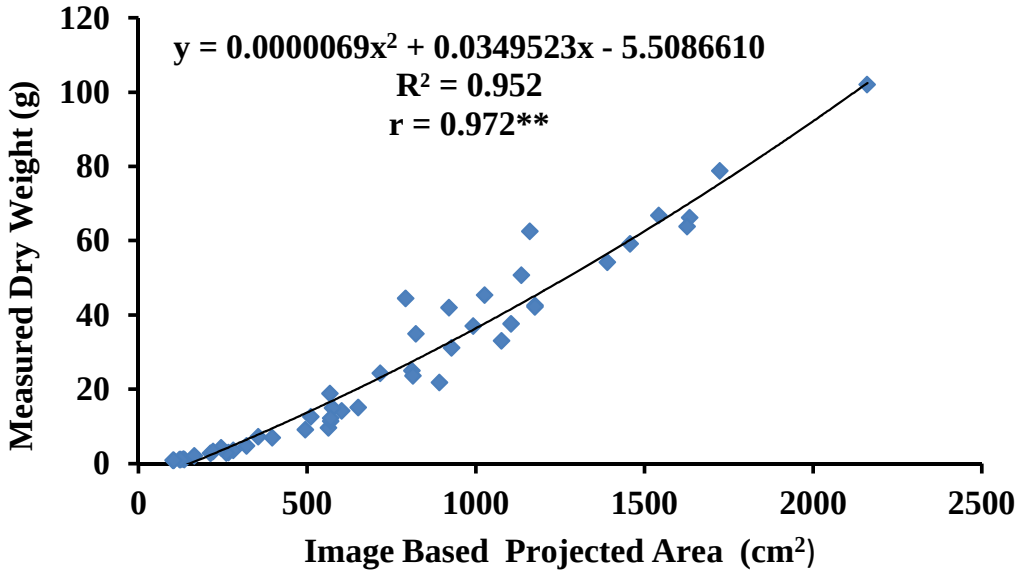

Fig 17(b): Nonlinear relationship between dry weights measured by destructive sampling and image based projected area

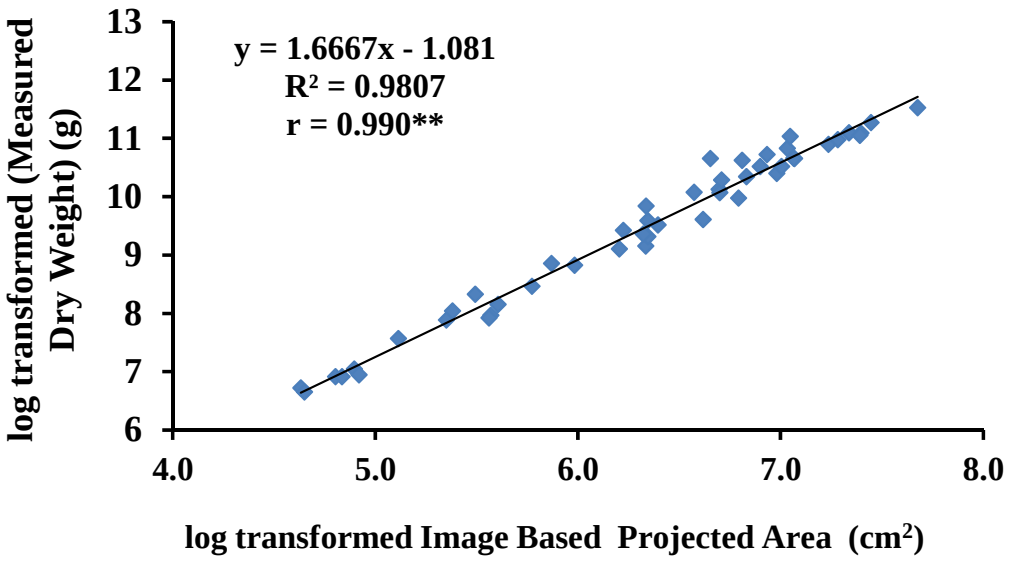

Fig.17(c): Log-log relationship between dry weights measured by destructive sampling and image based projected area

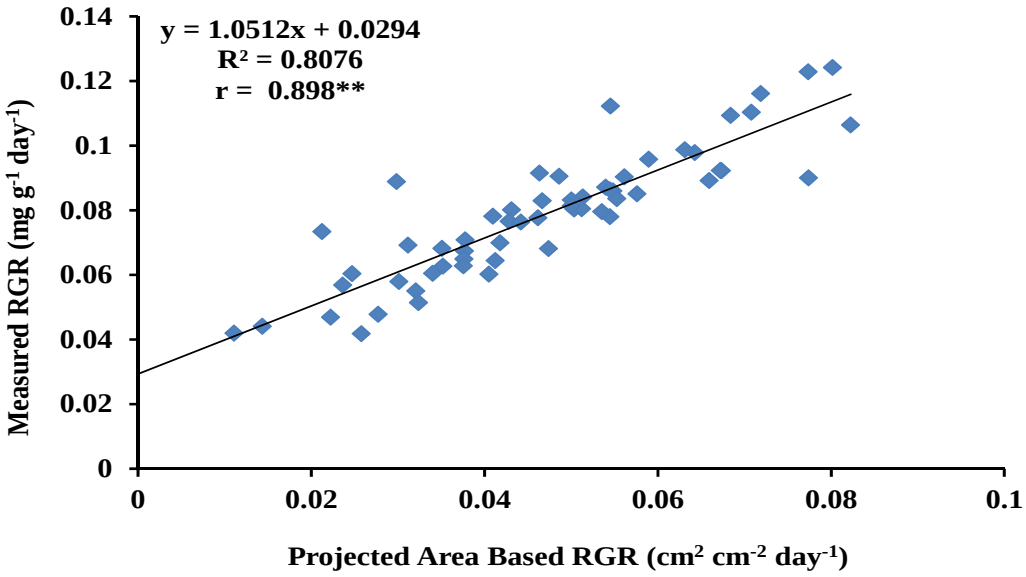

Fig.18: Correlation between RGR measured by destructive sampling and RGR from image based projected area

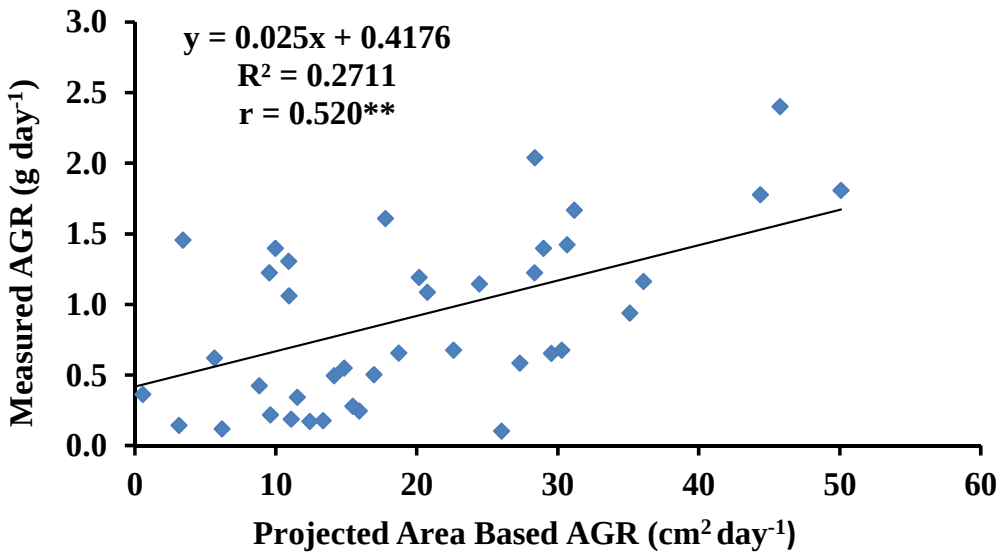

Fig.19: Correlation between AGR measured by destructive sampling and AGR from image based projected area

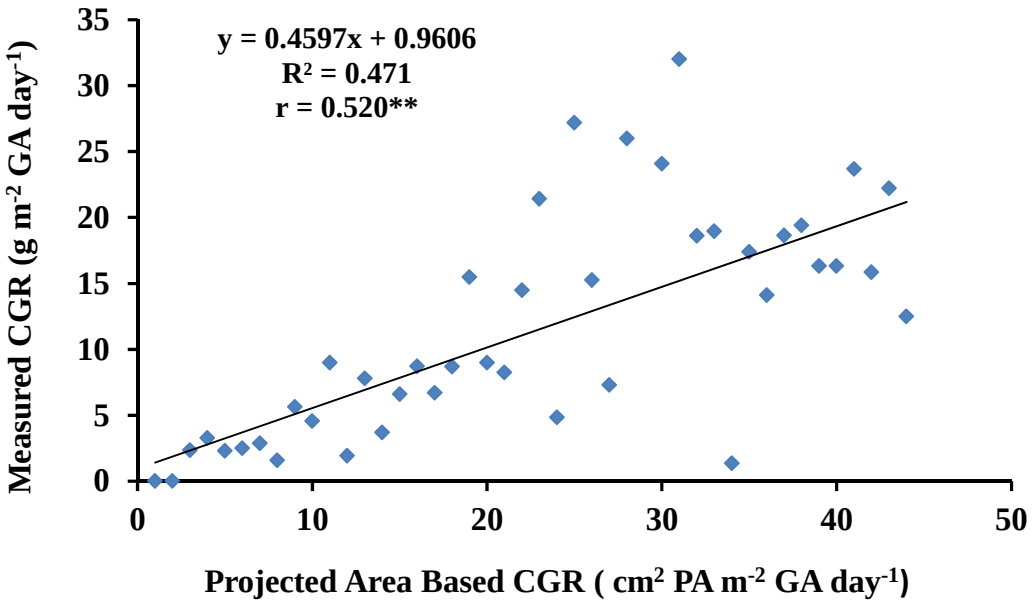

Fig.20: Correlation between CGR measured by destructive sampling and CGR from image based projected area

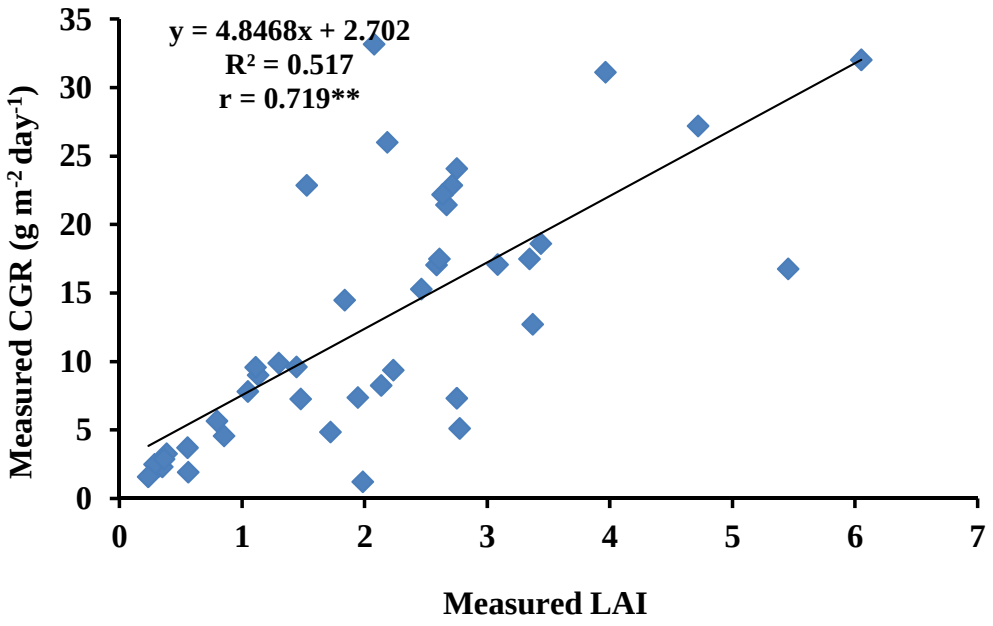

Fig.21: Correlation between measured CGR and measured LAI

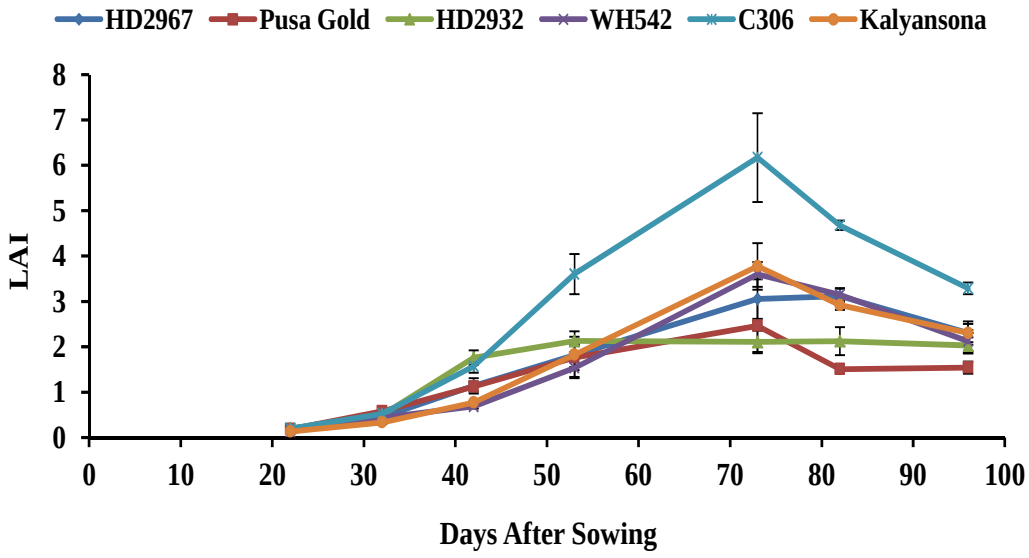

Fig.22: Progress of LAI at different DAS in six wheat genotypes

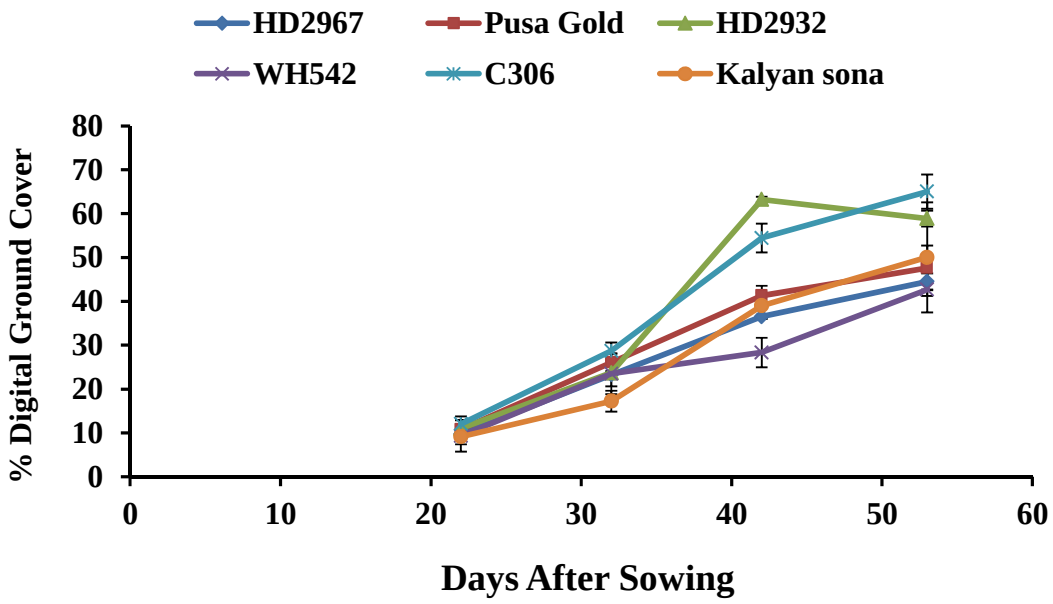

Fig.23(a): Progress of % digital ground cover at different DAS in six wheat genotypes

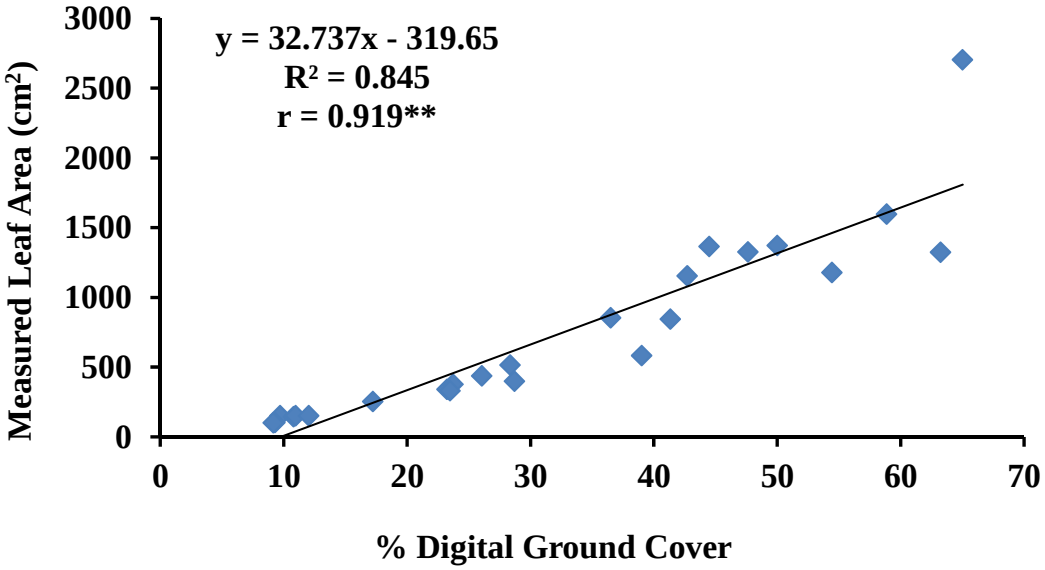

Fig.23(b): Correlation between % digital ground cover and measured leaf area

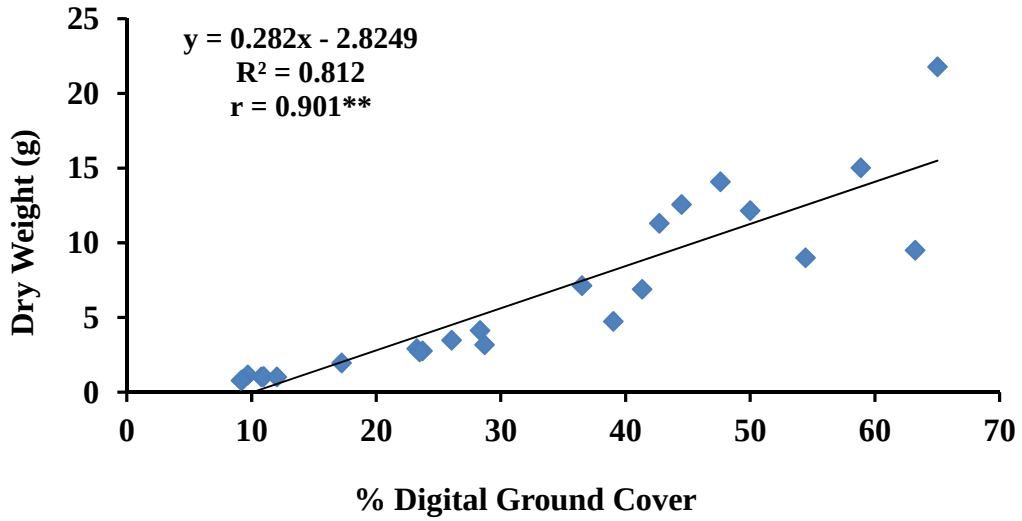

Fig.23(c): Correlation between % digital ground cover and dry weight

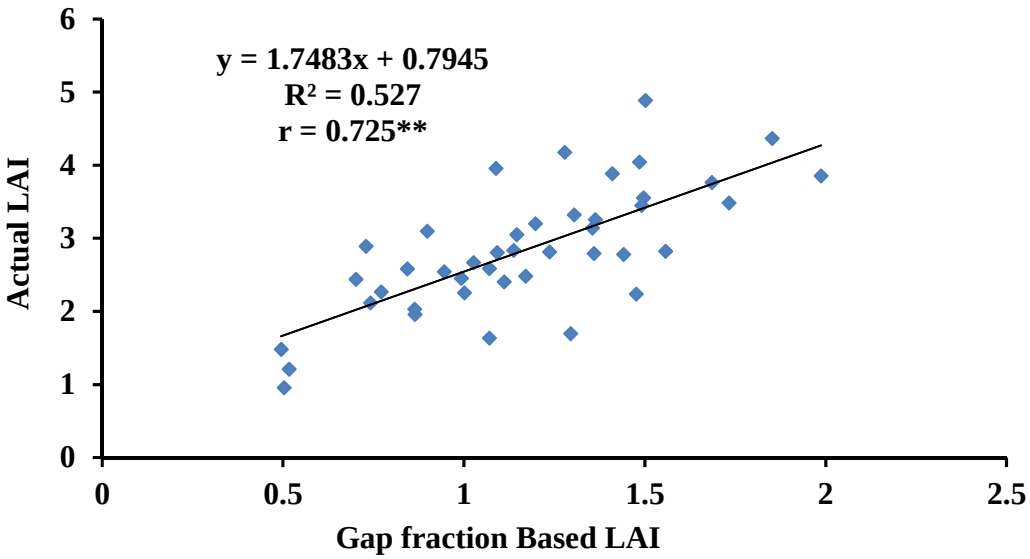

Fig.24(a): Correlation between actual LAI and gap fraction based LAI

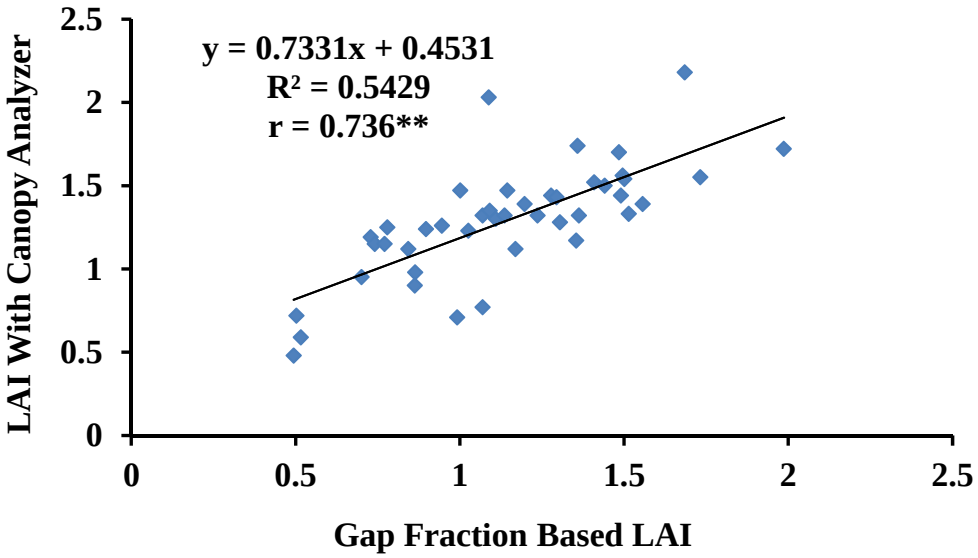

Fig.24(b): Correlation between LAI with canopy analyzer and gap fraction based LAI

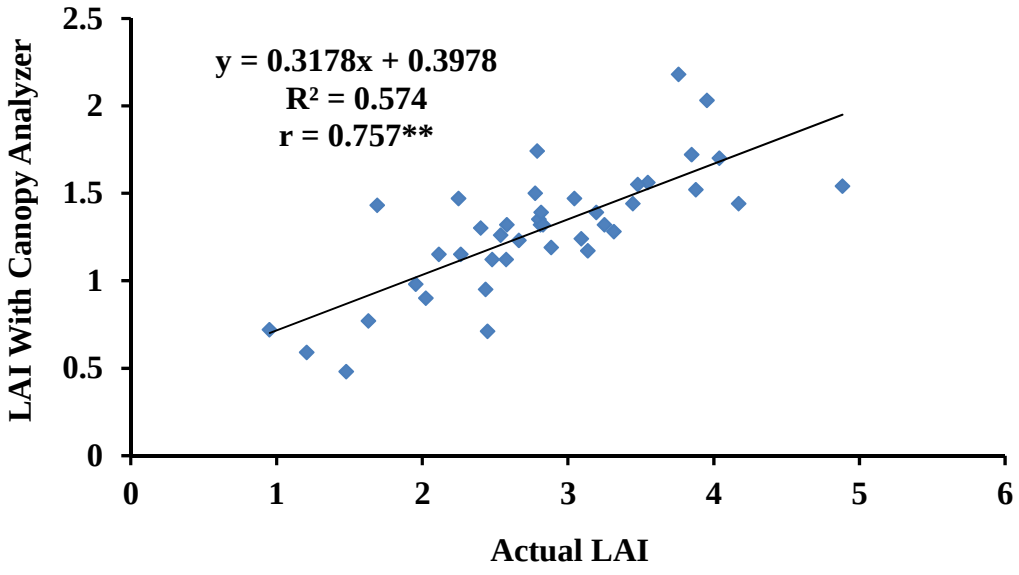

Fig.24(c): Correlation between LAI with canopy analyzer and actual LAI

Table 5: LAI at different DAS from 30 cm row length of crop in six wheat genotypes

Wheat genotypes	Day after sowing						
	22	32	42	53	73	82	96
HD2967	0.202	0.453	1.138	1.819	3.053	3.119	2.304
Pusa Gold	0.189	0.582	1.125	1.766	2.463	1.512	1.545
HD2932	0.202	0.502	1.763	2.130	2.107	2.125	2.031
WH542	0.136	0.441	0.685	1.538	3.598	3.147	2.126
C306	0.200	0.529	1.569	3.605	6.171	4.677	3.287
Kalyansona	0.134	0.337	0.775	1.827	3.775	2.919	2.305
Mean	0.177	0.474	1.176	2.114	3.528	2.916	2.266
CD at 5%	0.054	N/A	0.304	1.15	1.659	0.495	0.685
CV (%)	16.576	18.115	14.048	29.515	25.527	9.206	16.397

Table 6: % Digital Ground Cover at different DAS from 30 cm row length of crop in six wheat genotypes

Wheat genotypes	Days after sowing			
	22	32	42	53
HD2967	9.720	23.244	36.503	44.497
Pusa Gold	10.803	26.069	41.335	47.621
HD2932	10.978	23.725	63.235	58.882
WH542	9.305	23.485	28.345	42.710
C306	12.039	28.714	54.447	65.025
Kalyansona	9.162	17.227	39.025	50.018
Mean	10.334	23.744	43.815	51.459
CD at 5%	N/A	N/A	7.995	N/A
CV (%)	26.461	21.413	9.902	20.646

4.4.1.2. Total Carotenoid content

The carotenoid content at different DAS in six wheat genotypes is shown in (**Table8**). The carotenoids were found highest at 96 DAS stage. The highest carotenoids were observed in wheat genotype Kalyansona at 96 DAS stage. This genotype was not significantly different over the other genotypes. There was significant difference between the genotypes for carotenoids at 63 and 82 DAS. But, there was no significant difference between the genotypes for carotenoids at 22, 32, 42, 53, 73 and 96 DAS.

4.4.2. Chlorophyll and carotenoid content on dry weight basis

4.4.2.1. Total chlorophyll content

The total chlorophyll content at different DAS in six wheat genotypes is shown in (**Table9**). The mean total chlorophyll was found highest at 42 DAS stage. The highest total chlorophyll content was observed in wheat genotype C306 at 22 DAS stage. Although this variety showed highest total chlorophyll but the varietal differences were not significant. There was significant difference between the genotypes for total chlorophyll at 53 DAS. But, there was no significant difference between the genotypes for total chlorophyll at 22, 32, 42, 63, 73, 82 and 96 DAS.

4.4.2.2. Total Carotenoid content

The carotenoid content at different DAS in six wheat genotypes is shown in (**Table10**). The mean carotenoid content was found highest at 42 DAS stage. The highest carotenoid content was observed in wheat genotype HD2932 at 42 DAS stage. However, this genotype was not significantly different over the other genotypes. There was significant difference between the genotypes for carotenoids at 73 DAS. But, there was no significant difference between the genotypes for carotenoids at 22, 32, 42, 53, 63, 82 and 96 DAS.

Table 7: Total Chlorophyll content (mg g^{-1} fw) at different DAS in six wheat genotypes

Wheat genotypes	Day after sowing							
	22	32	42	53	63	73	82	96
HD2967	1.590	1.571	2.065	1.683	1.654	2.572	2.419	2.639
Pusa Gold	1.700	1.325	2.195	1.601	1.889	1.892	1.849	2.881
HD2932	1.295	1.311	2.092	1.727	1.766	2.227	2.528	2.155
WH542	1.592	1.328	1.779	1.239	1.914	1.883	2.606	2.453
C306	1.290	1.686	1.891	1.439	1.485	1.960	2.114	2.596
Kalyansona	1.148	1.411	2.293	1.751	1.662	2.043	2.744	2.836
Mean	1.436	1.439	2.053	1.573	1.728	2.096	2.377	2.593
CD at 5%	N/A	N/A	N/A	N/A	N/A	0.415	N/A	N/A
CV (%)	13.594	11.723	13.657	11.340	15.912	9.476	12.070	13.594

Table 8: Total Carotenoid content (mg g^{-1} fw) at different DAS in six wheat genotypes

Wheat genotypes	Day after sowing							
	22	32	42	53	63	73	82	96
HD2967	0.384	0.435	0.572	0.447	0.473	0.663	0.633	0.666
Pusa Gold	0.411	0.356	0.583	0.438	0.579	0.534	0.449	0.677
HD2932	0.333	0.386	0.603	0.476	0.614	0.580	0.614	0.542
WH542	0.389	0.374	0.533	0.346	0.514	0.491	0.658	0.575
C306	0.320	0.467	0.498	0.389	0.496	0.563	0.502	0.613
Kalyansona	0.296	0.386	0.588	0.457	0.507	0.609	0.600	0.716
Mean	0.356	0.401	0.563	0.426	0.531	0.573	0.576	0.631
CD at 5%	N/A	N/A	N/A	N/A	0.079	N/A	0.072	N/A
CV (%)	21.412	14.572	10.132	13.135	8.113	14.261	6.758	12.943

Table 9: Total Chlorophyll content (mg g^{-1} dw) at different DAS in six wheat genotypes

Wheat genotypes	Day after sowing							
	22	32	42	53	63	73	82	96
HD2967	13.554	6.711	12.608	12.067	8.478	11.018	8.786	9.275
Pusa Gold	15.621	6.188	15.172	9.594	7.699	7.951	8.622	8.934
HD2932	10.354	4.961	13.944	11.545	6.823	10.375	9.383	9.487
WH542	12.177	4.718	11.517	9.780	9.800	7.918	10.093	9.886
C306	17.426	4.793	13.742	11.942	6.179	9.257	10.405	10.636
Kalyansona	9.509	5.392	16.014	15.029	8.884	8.809	10.373	10.438
Mean	13.107	5.460	13.833	11.659	7.977	9.221	9.610	9.776
CD at 5%	N/A	N/A	N/A	2.867	N/A	N/A	N/A	N/A
CV (%)	29.828	18.804	17.294	13.345	16.983	15.375	13.107	13.676

Table 10: Total Carotenoid content (mg g^{-1} dw) at different DAS in six wheat genotypes

Wheat genotypes	Day after sowing							
	22	32	42	53	63	73	82	96
HD2967	1.494	1.571	2.670	2.160	1.864	2.349	1.978	1.931
Pusa Gold	1.817	1.267	2.836	2.012	2.030	1.906	1.637	1.698
HD2932	1.502	1.276	2.904	2.414	2.098	2.214	1.920	1.834
WH542	1.623	1.126	2.616	1.929	2.069	1.743	2.063	1.869
C306	1.062	1.180	2.467	1.965	1.801	2.201	1.903	1.870
Kalyansona	1.342	1.258	2.889	2.230	2.165	2.243	1.674	2.051
Mean	1.474	1.280	2.730	2.118	2.005	2.109	1.862	1.876
CD at 5%	N/A	N/A	N/A	N/A	N/A	0.283	N/A	N/A
CV (%)	19.289	12.949	12.571	11.761	11.169	8.256	8.980	19.289

Chapter 5

DISCUSSION

5.1. Dry matter production and its relationship with image based projected area

Crop growth represents increase in biomass and leaf area and it is one of the most important representative trait of crop performance. Better canopy growth in term of biomass accumulation and leaf area production is visible through extent of ground cover (Mullan and Reynolds, 2010). Estimation of canopy growth by traditional method requires destructive sampling for biomass and leaf area. It requires more time, labour and one can't measure any parameter again. Presently there are phenotyping methods available for biomass estimation based on visible images, NIR images and fluorescence imaging under controlled and field conditions [Fiorani and Schurr (2013), Araus and Cairns (2014), Li *et al.* (2014)].

In the present study the above-ground plant dry weight (g) from 30 cm row length from 20 to 96 DAS in six wheat genotypes was estimated by destructive sampling and indirectly by projected area measurement. In general, there was a similar pattern of increase in dry matter and projected area (**Fig.5, 7, 9, 11, 13, 15**). For example, the biomass and projected area was less at initial stage and increased later. Also at the 96 DAS the highest biomass and projected area was measured in the variety C306. Similarly the lowest aboveground plant dry weight and projected area was observed in genotype HD2967 at this stage (**Fig.5**). The reports on image based phenotyping of biomass under field conditions also show that digital photography is a promising approach that enables estimation of green biomass, soil cover, plant color etc. Casadesus *et al.* (2007). Paruelo *et al.* (2000) studied above-ground plant biomass using a photographic technique. Lee *et al.* (2013) used digital camera image analysis for estimation of rice growth and nitrogen nutrition status. Hunt *et al.* (2015) used a custom-made high-throughput image analysis tool for estimation of dry matter production of individual perennial ryegrass in field. The image analysis tool captured 25% more of the variation, than those from visual growth scores. Use of both the Visible and NIR images from digital cameras can be helpful in estimation of NDVI which is associated with biomass and crop growth. Recently, Greider *et. al.* (2015)

estimated RGR in wheat non-destructively under field conditions using NDVI canopy cover images. Sakamoto *et al.* (2012) used camera observation system for monitoring crop growth of maize and soybean in field. Dammer *et al.* (2016) made on-the-go phenotyping in field potatoes using camera vision and showed that it helped identifying areas showing different plant growth and differences in the temporal development of the crop.

Similar use of visible image based projected area for biomass estimation has been done earlier under controlled conditions by many workers. The RGB imaging is the basic component of presently available high throughput phenotyping platforms. These studies are as follows – Leister *et al.* (1999) were the first to study plant growth in *Arabidopsis thaliana* by non-invasive image analysis under controlled environment. Top view image based plant area estimation was correlated fresh weight. Walter *et al.* (2007) studied the dynamics of seedling growth from images in tobacco and Arabidopsis under controlled environment and rapid detection of genetic and environmental parameters regulating plant growth was possible. Golzarian *et. al.* (2011) estimated shoot biomass of cereal plants from their two dimensional images as a linear function of the projected shoot area of plants in the images. Berger *et al.* (2012) has also provided protocol to estimate biomass and growth assuming relation between biomass and projected area for a growth phenotyping pipeline for *Arabidopsis thaliana* using platform of LemnaTec 3D Scanalyzer system, Germany. Arvidsson *et al.* (2011) described a growth phenotyping pipeline for *Arabidopsis thaliana* with capacity to phenotype rosette area of 7000 plants/day by RGB image using the parameters of area, convex hull and compactness. The study quantified genotype effects on total rosette area and relative leaf growth rate (RLGR). Junker *et al.* (2014) observed significant correlation between fresh biomass and estimated volume of 63 maize inbred lines grown in various growth conditions. Fahlgren *et al.* (2015) observed phenotyped biomass and growth rates in wild *Setaria viridis* and domesticated *Setaria italica* under controlled-environment. Chen *et al.* (2016) predicted barley plant biomass from image-derived parameters and they observed that plant biomass could be accurately predicted from images using a random forest model. Hairmansis *et al.* (2014) studied rice for total shoot area and senescent shoot area, calculated from visible red-green-blue (RGB) and fluorescence images for biomass estimation. Flood *et al.* (2016) studied growth and reflectance in *Arabidopsis*

thaliana using an automated high-throughput phenotyping platform, the Phenovator, capable of screening 1440 Arabidopsis plants multiple times per day. Fluctuations in PLA between day and night were captured emphasizing the importance of frequent measurements and change in leaf angle in light and dark.

Based on these associations, the present study could find a significantly higher correlation between actual dry biomass and image based projected area. This association was having a very high coefficient of determination for linear, non linear and log-log relations. For instance, the correlation between measured dry weight and image based projected area parameter was highly significant (r = 0.972**, **Fig.17a**) with R^2 value (0.945) for linear relationship (y = 0.0476x - 9.352). For non linear relationship (y = $0.0000069x^2$ + 0.034x - 5.508) the R^2 value increased to 0.952 (**Fig.17b**). The correlation between log-log measured dry weight and image based projected area parameters further increased to (r = 0.99**, **Fig.17c**) with R^2 value (0.98) for log-log relationship (y = 1.6667x - 1.08). Therefore these equations can be useful for prediction of biomass from projected area.

The projected area was further used to calculate Relative Growth rate (RGR), Crop Growth Rate (CGR) and Average Growth Rate (AGR) based on the projected area. The present study also found significant correlation between the estimates of dry weight based relative growth rate (RGR) and projected area based RGR (r = 0.898**, **Fig.18**). There was a linear relationship between these with a high R^2 value (0.807, y = 1.0512x + 0.0294). A significant correlation was also observed between the estimates of dry weight based Crop Growth Rate (CGR) and projected area based CGR (r = 0.520**, **Fig.20**). There was a linear relationship between these with a high R^2 value (0.471, y = 0.4597x + 0.9606). A significant correlation was also observed between the estimates of dry weight based Average Growth Rate (AGR) and projected area based AGR (r = 0.520**, **Fig.19**). There was a linear relationship between these with a R^2 value (0.27, y = 0.025x + 0.417). These relations can be useful for prediction of RGR, CGR and AGR from projected area. The prediction would be best for RGR followed by CGR and AGR.

Some studies which have provided correlation coefficient and coefficient of determination for their estimates of biomass and growth parameters are as follows. Tomasel *et al.* (2001) studied chromaticity-based technique for estimation of

above-ground plant biomass from a short-grass steppe and showed high correlation between pixel count and measured values of green biomass (r = 0.95). Casadesús and Villegas (2014) estimated leaf area index and biomass using conventional digital cameras. The image derived index pertaining to the fraction of green pixels over the total pixels of the image showed good correlations with all biomass variables and was robust to lighting conditions. Jia *et al.* (2014) used digital images to monitor the growth of cotton crop in field and observed that the canopy cover and above-ground biomass were closely related (R^2 = 0.74-0.94). Kefauver *et al.* (2015) measured RGB picture vegetation indexes from field grown maize. The RGB picture vegetation indexes outperformed NDVI with R^2 values up to 0.65, compared to 0.56 for NDVI. Hoyos-Villeg *et al.* (2014) used common digital cameras and estimated canopy cover, total above-ground biomass, leaf biomass in soybean. High correlation between the ground cover data (image analysis) and crop growth rate was observed (R^2 = 0.69). Tackenberg (2007) studied biomass, growth rates, vertical biomass distribution and dry matter content using scaled digital images under controlled greenhouse in twenty-seven annual and perennial grass species (Poaceae). They observed a high correlation between log-log relation of dry matter and projected area.

In many studies a combination of visible and fluorescence images has been used for estimation of biomass based on the digital volume parameters which combines top view and side view image parameters to improve the biomass estimation. These studies include - Klukas *et al.* (2014) who found that in general the correlation of fluorescence image based digital volume showed a higher correlation with fresh weight and dry weight compared to visible image based digital volume. Honsdorf *et al.* (2014) found a high correlation (r = 0.98) between image based biomass estimates and actual biomass in barley under controlled environment. Neilson *et al.* (2015) found a strong positive correlation between projected leaf area and above-ground biomass, height, and true leaf area. The RGR output showed significant correlation with the RGR by traditional destructive harvests. Parent *et al.* (2015) also found that observed and measured biomass were highly correlated ($P<0.001$). Neumann *et al.* (2015) imaged the top view and side view for estimation of plant volume in barley under controlled environment and found good association between destructively measured plant fresh weight and digital biomass ($R^2 > 0.9$). Chen *et al.* (2014) studied the phenotypic components of crop plant growth and

drought responses in barley under controlled environment. Digital volume showed the best correlation with manually measured fresh weight and dry weight and logistic model simulated biomass accumulation better (r = 0.89). Dhondt *et al.* (2014) studied time-resolved imaging of *in vitro Arabidopsis* rosette growth and found that mutants revealed specificities in growth behavior. Humplík *et al.* (2015) reported that digital RGB image analysis helped in correlation between green area and biomass. Bac-Molenaar *et al.* (2015) also reported that fresh weight in Arabidopsis was positively correlated with projected leaf area (PLA) after 14 days (r>0.95). Edlich-Muth *et al.* (2016) found that twenty image features explained 73% of the variance in hybrid fresh weight. Cabrera-Bosquet *et al.* (2016) studied radiation-use efficiency of thousands of plants in a phenotyping platform based on the estimation of leaf area and fresh plant weight from images and found a high correlation between biomass accumulation and intercepted PPFD.

5.2. Canopy growth and its relation with Digital Ground Cover (DGC) in wheat genotypes

The leaf area from 30 cm row length of crop (or the equivalent LAI) measured by destructive sampling was found highest at 73 DAS stage before anthesis. Fischer (1983) also stated that leaf area increases progressively until flag leaf formation. At this stage the highest leaf area was observed in wheat genotype C306. Also there was significant difference between the genotypes for leaf area index at 22, 42, 53, 73, 82 and 96 DAS (**Table 5, Fig.22**). A high correlation was observed between CGR and LAI (**Fig.21**). Fischer (1983) reported that CGR increases to maximum at LAI values of 6. This was also observed in C306 as it had a highest LAI of 6.17 at 73 DAS and also a highest CGR value of 31.56 g m^{-2} day^{-1} between 63-73 DAS (**Table 5**).

Digital image analysis of photographs to measure digital ground cover helps in quantitatively measuring the green vegetation from the total ground area (Mullan and Reynolds 2010 and Mullan *et al.* 2012). The % digital ground cover at different DAS from 30 cm row length of crop in six wheat genotypes is shown in [**Fig.23 (a)**]. The % digital ground cover was found highest at 53 DAS stage in wheat genotype C306 (**Table 6**). However, it was not significantly different over the other genotypes. There was significant difference between the genotypes for % digital ground cover at 42 DAS. But, there was also no significant difference between the genotypes for %

digital ground cover at 22 and 32 DAS. The correlation between measured leaf area and % digital ground cover parameter [**Fig.23(b)**] was highly significant (r = 0.919**). Also, there linear relationship between these have a high R^2 value (0.845, y = 32.737x - 319.65) which can be useful for prediction of leaf area % from digital ground cover. Campillo *et al*. (2010) estimated the LAI in vegetable crops by using digital images. The percentage of groundcover (PGC) and measured LAI were highly correlated (R^2 > 0.88). Mullan and Reynolds (2010) also observed a R^2 of 0.80 between DGC and LAI in wheat. Similarly, there was high correlation between measured dry weight and % digital ground cover [**Fig.23(c)**]. It shows a highly significant correlation (r = 0.901**) and a linear relationship with high R^2 value (0.812, y = 0.282x - 2.8249) which can be useful for prediction of dry weight from % digital ground cover. Mullan and Reynolds (2010) also observed a R^2 of 0.63 between DGC and dry matter production in wheat. Pandey *et al*. (2016) also observed a high correlation between canopy cover and biomass at anthesis in juncea canola hybrids.

5.3. Canopy growth and estimation of LAI using gap fraction in wheat genotypes

One of the important and most widely used methods of estimating canopy growth is estimation of gap fraction which can be described as the fraction of view that is not blocked by foliage (Welles 1990, Andrieu and Baret 1993, Welles and Cohen 1996, Weiss 2004). In the present study the images taken at zenith angle 57.5° with mobile phone were analyzed for gap fraction. Comparisons of these with the LAI 2000 canopy analyzer lead to significant correlations. For instance, the correlation between actual LAI and gap fraction based LAI [**Fig.24(a)**] was significant (r = 0.725**) and there was a linear relationship between these having a high R^2 value (0.527, y = 1.7483x + 0.7945). Similarly, correlation between LAI with canopy analyzer and gap fraction based LAI [**Fig.24(b)**] was also highly significant (r = 0.736**) with a linear relationship and a high R^2 value (0.542, y = 0.7331x + 0.4531). The correlation between LAI measure with canopy analyzer and actual LAI parameter measured by destructive sampling [**Fig.24(c)**] was also highly significant (r = 0.757**) with a linear relationship (R^2 = 0.574, y = 0.3178x + 0.3978). Some of the similar studies using gap fraction analysis from images were Demarez *et al.* (2008), Liu and Pattey (2010), Baret *et al*. (2010), Liu *et al.* (2013) and Confalonieri *et al*. (2013). These

showed that images taken at zenith angle 57.5° can be very useful for non destructive LAI estimation and are comparable to the estimations made by canopy analyzer.

Chapter 6

SUMMARY AND CONCLUSION

A study was conducted to estimatebiomass and crop growth in wheat with the help of non-destructive image based phenotyping methods. Six wheat genotypes (viz. HD2967, Pusa Gold, HD2932, WH542, C306 and Kalyansona) differing in growth habit were grown in field with 3 replications in RBD design. Samples were taken from 30 cm row length of crops containing 17 plants. For biomass and growth estimation the images of side view as well as top view of canopy were taken by a customized set-up/apparatus with digital camera. The side view images were analyzed in ImageJ for estimation of projected area.The top view of canopy was used to estimate Digital Ground Cover (DGC) with Photoshop software. In another experiment, images of bottom to top view of canopy were taken by mobile at 57^{o} angle from zenith and analyzed for gap fraction. Samples from the same place were cut and measured for leaf area.

The results from above experiments are summarized as follows -

- The dry matter production and image based projected area followed similar pattern of increase from 22 DAS to 96 DAS in all six wheat genotypes.
- The correlation between measured dry weight and image based projected area parameter showed a highly significant correlation (r = 0.972**). Also, linear relationship between these parameters has a high R^2 value (0.945) which can be useful for prediction of biomass from image based projected area. Similarly the log–log transformed biomass and projected area was also highly correlated (r = 0.99**, with linear relationship R^2= 0.980).
- The correlation between dry weight based measured RGR and projected area based RGR parameter shows a highly significant correlation (r = 0.898**). Also, there was a linear relationship between these with a high R^2 value (0.807) which can be useful for prediction of RGR from projected area based RGR.

- The correlation between dry weight based AGR and projected area based AGR parameter shows a highly significant correlation (r = 0.520**). Also, there linear relationship between these have a high R^2 value (0.271) which can be useful for prediction of AGR from projected area based AGR.
- The correlation between dry weight based CGR and projected area based CGR parameter shows a highly significant correlation (r = 0.520**). Also, there linear relationship between these have a high R^2 value (0.471) which can be useful for prediction of CGR from projected area based CGR.
- The correlation between measured leaf area and % DGC parameter shows a highly significant correlation (r = 0.919**). Also, there linear relationship between these have a high R^2 value (0.845) which can be useful for prediction of leaf area from %digital ground cover.
- The correlation between measured dry weight and % digital ground cover parameter shows a highly significant correlation (r = 0.901**). Also, there linear relationship between these have a high R^2 value (0.812) which can be useful for prediction of dry weight from % digital ground cover.
- The correlation between actual LAI and gap fraction based LAI parameter shows a high correlation (r = 0.725**). Also, there linear relationship between these have a high R^2 value (0.527) which can be useful for prediction of actual LAI from projected area based LAI.
- The correlation between LAI with canopy analyzer and gap fraction based LAI parameter shows a highly significant correlation (r = 0.736**). Also, there linear relationship between these have a high R^2 value (0.542) which can be useful for prediction of LAI from projected area based LAI.
- The correlation between LAI measure with canopy analyzer and actual LAI shows a highly significant correlation (r = 0.757**). Also, there is a linear relationship between these with a high R^2 value (0.574).

From above results it can be concluded that –

- The biomass of wheat can be estimated indirectly from image based projected area of side view of crop.
- The growth parameters (RGR, CGR and AGR) can be estimated from image projected area.

- The digital ground cover from top view images is related to plant biomass and leaf area.
- Gap fraction analysis of bottom to top view images by mobile camera can be used for LAI estimation.

Image based phenotyping of crop growth in wheat

ABSTRACT

Biomass production is one of the most important traits governing crop production. Future increases in yield potential of wheat will require enhancing the biomass. The present study investigated the image based non destructive estimation of biomass and crop growth in wheat. Six wheat genotypes (viz. HD2967, Pusa Gold, HD2932, WH542, C306 and Kalyansona) were grown in field with 3 replications in RBD design. For biomass and canopy growth estimation, side view images as well as top view (from 30 cm row) were taken by a customized set-up / apparatus with digital camera. The images were analyzed in ImageJ to measure projected area. The results showed that the dry matter production and image based projected area followed similar pattern of increase from 22 DAS to 96 DAS in all six wheat genotypes. There was a highly significant correlation between measured dry weight and image based projected area ($r = 0.972^{**}$, with linear relationship $R^2 = 0.945$). Similarly the log-log transformed biomass and projected area was also highly correlated ($r = 0.99^{**}$, with linear relationship $R^2 = 0.980$). These relationships can be used for prediction of biomass from image based projected area. There was also a high correlation between dry weight and projected area based growth parameters i.e. Relative Growth Rate - RGR ($r = 0.8985^{**}$), Crop Growth Rate - CGR ($r = 0.520^{**}$) and Average Growth Rate - AGR ($r = 0.520^{**}$). Based on the top view images analyzed in Photoshop, the measured leaf area and dry matter showed a highly significant correlation with % Digital Ground Cover - DGC ($r = 0.919^{**}$ and 0.901^{**} respectively). In another experiment, images of bottom to top view of canopy were taken by mobile at 57^{o} angle from zenith and analyzed for gap fraction. The actual Leaf Area Index (LAI) and gap fraction based LAI showed a high correlation ($r = 0.725^{**}$). The LAI measured with canopy analyzer instrument (LAI 2000, LiCor) and gap fraction based LAI parameter from mobile camera also showed a highly significant correlation ($r = 0.736^{**}$). From the above results it can be concluded that the biomass of wheat can be estimated indirectly from image based projected area of side view of crop. The growth parameters (RGR, CGR and AGR) can be similarly estimated. The estimation of digital ground cover from top view images can also be used to estimate to plant biomass and leaf area. Also, the gap fraction analysis of bottom to top view images by mobile camera can be used for LAI estimation.

गेहूँ में फसल वृद्धि का छायाचित्र आधारित लक्षणप्ररूपण

सारांश

जैविक भार उत्पादन फसल की उत्पादन क्षमता को निर्धारित करने वाला एक अति महत्वपूर्ण गुण है । भविष्य में गेहूँ की उत्पादन क्षमता बढ़ाने हेतु जैविक भार को बढ़ाना होगा । प्रस्तुत अध्ययन में, गेहूँ में छायाचित्र आधारित अभिरंजक विधि द्वारा जैविक भार एवं फसल वृद्धि का आकलन किया गया । गेहूँ की छः प्रजातियों (एच डी 2967, पूसा गोल्ड, डब्ल्यू एच 542, सी 306 एवं कल्याणसोना) को प्रक्षेत्र में तीन स्थानों पर रेंडमाइज्ड ब्लॉक डिजाइन में उगाया गया । जैविक भार एवं फसल कैनोपी के आकलन हेतू गेहूँ की फसल की पंक्तियों के बीच पार्श्व भाग एवं ऊपर से (30 से.मी. पंक्ति से) एक डिजिटल कैमरा युक्त स्वनिर्मित यंत्र से किया गया । छायाचित्रों का विश्लेषण 'इमेज जे' नामक सॉफ्टवेयर से किया एवं प्रक्षेपित क्षेत्रफल का मापन किया गया ।

परिणामों में ये पाया गया कि गेहूँ की छः प्रजातियों में 22 से 96 दिनों के बीच जैवभार उत्पादन एवं प्रक्षेपित क्षेत्रफल की बढ़वार में समरूपता थी । मापे गए जैव भार एवं प्रक्षेपित क्षेत्रफल में उच्च सह संबंध ($r = 0.972^{**}$ एवं रैखिक संबंध $R^2 = 0.945$) था । इसी प्रकार इनके लघुगणको में भी उच्च सहसम्बन्ध रहा ($r = 0.990^{*}$ एवं रैखिक सम्बन्ध $R^2 = 0.980$). इन समीकरणों से प्रक्षेपित क्षेत्रफल द्वारा जैव भार का आकलन किया जा सकता हैं । इसी प्रकार जैव भार एवं प्रक्षेपित क्षेत्रफल द्वारा आँकें गए वृध्दि मानकों में सह सम्बन्ध रहा जैसे - रिलेटिव ग्रोथ रेट - आर जी आर ($r = 0.895^{**}$), क्रोप ग्रोथ रेट - सी जी आर. ($r = 0.520^{**}$) एवं एवरेज ग्रोथ रेट - ए जी आर ($r = 0.520^{**}$). ऊपरी छायाचित्रों का फोटोशॉप सॉफ्टवेयर में विश्लेषण करने पर यह पाया गया कि - मापे गए पर्ण क्षेत्रफल एवं जैव भार एवं डिजिटल ग्राउंड कवर में उच्च सह सम्बन्ध था ($r = 0.919^{**}$ एवं 0.901^{**} क्रमवार). एक अन्य प्रयोग में कैनोपी का धरातल से ऊपरी ओर मोबाइल द्वारा 57° कोण पर छायाचित्र लिया गया । यह पाया गया कि मापे गए लीफ एरिया इंडेक्स (एल. ए. आई.) एवं कैनोपी गैप फ्रैक्शन में उच्च सह सम्बन्ध था ($r = 0.725^{**}$). इसी प्रकार कैनोपी एनालाइजर यंत्र (एल ए आई 2000) द्वारा मापे गए एल ए आई एवं मोबाइल कैमरा द्वारा मापे गए एल ए आई में उच्च सह सम्बन्ध था ($r = 0.736^{**}$).

उपरोक्त परिणामों के आधार पर यह निष्कर्ष आया कि - गेहूँ में जैव भार को अप्रत्यक्ष रूप से छायाचित्र के प्रक्षेपित क्षेत्रफल से आँका जा सकता है । इसी प्रकार पादप वृद्धि मानकों (आर जी आर, सी जी आर एवं ए जी आर) को मापा जा सकता है । ऊपरी छायाचित्रों से मापे गए डिजिटल ग्राउंड कवर द्वारा भी पादप जैव भार एवं पर्ण क्षेत्रफल का आकलन किया जा सकता है । इसके अतिरिक्त, मोबाइल कैमरा द्वारा लिए गए छायाचित्रों के गैप फ्रैक्शन का विश्लेषण करके भी लीफ एरिया इंडेक्स का आकलन किया जा सकता है ।

BIBLIOGRAPHY

Andrieu, B. and Baret, F. (1993). Indirect methods of estimating crop structure from optical measurements. C. Varlet-Grancher, R. Bonhomme, H. Sinoquet (Eds.), Crop Structure and Light Microclimate. Characterization and Applications, INRA Edition, Paris (1993), pp. 285–322

Arabidopsis Phenotyping: Assessment in Time and Space LemnaTec GmbH Matthias Eberius Pascalstr. 5952076 Aachen, Germany +49 2408 9383 102 matthias.eberius@lemnatec.de www.lemnatec.de LemnaTec moving field: Competitive phenotyping and microplots.

Araus, J.L. and Cairns, J.E. (2014). Field high-throughput phenotyping: The new crop breeding frontier. *Trends in Plant Science* **19**: 52-61.

Arvidsson, S., Pérez-Rodríguez, P. and Mueller-Roeber, B. (2011). A growth phenotyping pipeline for *Arabidopsis thaliana* integrating image analysis and rosette area modeling for robust quantification of genotype effects. *New Phytologist* **191**: 895-907.

Babar, M.A., Reynolds, M.P., Van Ginkel, M., Klatt, A.R., Raun, W.R. and Stone, M.L. (2006). Spectral reflectance to estimate genetic variation for in-season biomass, leaf chlorophyll, and canopy temperature in wheat. *Crop Science* **46**: 1046-1057.

Bac-Molenaar, J.A., Vreugdenhil, D., Granier, C. and Keurentjes, J.J. (2015). Genome-wide association mapping of growth dynamics detects time-specific and general quantitative trait loci. *Journal of Experimental Botany* DOI:10.1093/jxb/erv176.

Baret, F., De Solan, B., Lopez-Lozano, R., Ma, K. and Weiss, M. (2010). GAI estimates of row crops from downward looking digital photos taken perpendicular to rows at 57.5 zenith angle: Theoretical considerations based on 3D architecture models and application to wheat crops. *Agricultural and Forest Meteorology* **150**: 1393-1401.

Bartelink, H.H. (1997). Allometric relationships for biomass and leaf area of beech (Fagus sylvatica L). In *Annales des Sciences Forestieres* (Vol. 54, No. 1, pp. 39-50). EDP Sciences.

Bendig, J., Bolten, A., Bennertz, S., Broscheit, J., Eichfuss, S. and Bareth, G. (2014). Estimating biomass of barley using crop surface models (CSMs) derived from UAV-based RGB imaging. *Remote Sensing* **6**: 10395-10412.

Bendig, J., Yu, K., Aasen, H., Bolten, A., Bennertz, S., Broscheit, J., Gnyp, M.L. and Bareth, G. (2015). Combining UAV-based plant height from crop surface models, visible, and near infrared vegetation indices for biomass monitoring in barley. *International Journal of Applied Earth Observation and Geoinformation* **39**: 79-87.

Berger, B., de Regt, B. and Tester, M. (2012). High-throughput phenotyping of plant shoots. *Methods in Molecular Biology* **918**: 9-20.

Blackman, V.H. (1919). The compound interest law and plant growth. *Annals of Botany* **33**: 353-360.

Brown, S. (1997). Estimating biomass and biomass change of tropical forests: a primer. FAO For. Pap. 134.

Busemeyer, L., Mentrup, D., Möller, K., Wunder, E., Alheit, K., Hahn, V., Maurer, H.P., Reif, J.C., Würschum, T., Müller, J. and Rahe, F. (2013). Breedvision—A multi-sensor platform for non-destructive field-based phenotyping in plant breeding. *Sensors* **13**: 2830-2847.

Busemeyer, L., Ruckelshausen, A., Möller, K., Melchinger, A.E., Alheit, K.V., Maurer, H.P., Hahn, V., Weissmann, E.A., Reif, J.C. and Würschum, T. (2013). Precision phenotyping of biomass accumulation in triticale reveals temporal genetic patterns of regulation. *Scientific Reports* **3**: 2442.

Cabrera-Bosquet, L., Fournier, C., Brichet, N., Welcker, C., Suard, B. and Tardieu, F. (2016). High-throughput estimation of incident light, light interception and radiation-use efficiency of thousands of plants in a phenotyping platform. *New Phytologist* DOI: 10.1111/nph.14027.

Campillo, C., Garcia, M.I., Daza, C. and Prieto, M.H. (2010). Study of a non-destructive method for estimating the leaf area index in vegetable crops using digital images. *HortScience* **45**: 1459-1463.

Casadesus J, Kaya Y, Bort J, Nachit MM, Araus JL, Amor S and Villegas D (2007). Using vegetation indices derived from conventional digital cameras as selection criteria for wheat breeding in water-limited environments. *Annals of Applied Biology* **150:** 227-236.

Casadesús, J., and Villegas, D. (2014). Conventional digital cameras as a tool for assessing leaf area index and biomass for cereal breeding. *Journal of Integrative Plant Biology* **56**: 7–14.

Causton, D.R. and Venus, J.C. (1981). *The biometry of plant growth*. Edward Arnold.

Chapman, S.C., Merz, T., Chan, A., Jackway, P., Hrabar, S., Dreccer, M.F., Holland, E., Zheng, B., Ling, T.J. and Jimenez-Berni, J. (2014). Pheno-copter: a low-altitude, autonomous remote-sensing robotic helicopter for high-throughput field-based phenotyping. *Agronomy* **4**: 279-301.

Chen, D., Neumann, K., Friedel, S., Kilian, B., Chen, M., Altmann, T. and Klukas, C. (2014). Dissecting the phenotypic components of crop plant growth and drought responses based on high-throughput image analysis. *The Plant Cell* **26**: 4636-4655.

Chen, D., Shi, R., Pape, J.M. and Klukas, C. (2016). Predicting plant biomass accumulation from image-derived parameters. *BioRxiv*. Pp 046656.

Confalonieri, R., Foi, M., Casa, R., Aquaro, S., Tona, E., Peterle, M., Boldini, A., De Carli, G., Ferrari, A., Finotto, G. and Guarneri, T. (2013). Development of an app for estimating leaf area index using a smartphone. Trueness and precision determination and comparison with other indirect methods. *Computers and Electronics in Agriculture* **96**: 67-74.

Crain, J.L., Wei, Y., Barker, J., Thompson, S.M., Alderman, P.D., Reynolds, M., Zhang, N. and Poland, J. (2016). Development and deployment of a portable field phenotyping platform. *Crop Science* **56**: 965-975

Dammer, K.H., Dworak, V. and Selbeck, J. (2016). On-the-go phenotyping in field potatoes using camera vision. *Potato Research* First online: 23 January 2016

Demarez, V., Duthoit, S., Baret, F., Weiss, M. and Dedieu, G. (2008). Estimation of leaf area and clumping indexes of crops with hemispherical photographs. *Agricultural and Forest Meteorology* **148**: 644-655.

Dhondt, S., Gonzalez, N., Blomme, J., De Milde, L., Van Daele, T., Van Akoleyen, D., Storme, V., Coppens, F., TS Beemster, G. and Inzé, D. (2014). High-resolution time-resolved imaging of *in vitro* Arabidopsis rosette growth. *The Plant Journal* **80**: 172-184.

Eberius M. ( ). Arabidopsis Phenotyping: Assessment in time and space. LemnaTec GmbH, Pascalstr. 59, 52076 Aachen, Germany

Edlich-Muth, C., Muraya, M.M., Altmann, T. and Selbig, J. (2016). Phenomic prediction of maize hybrids. Biosystems. May 19. S0303-2647(16)30071-5. DOI: 10.1016/j.biosystems.2016.05.008.

Ehlert, D., Hammen, V. and Adamek, R. (2003). On-line sensor pendulum-meter for determination of plant mass. *Precision Agriculture* **4**: 139-148.

Ehlert, D., Heisig, M. and Adamek, R. (2010). Suitability of a laser rangefinder to characterize winter wheat. *Precision Agriculture* **11**: 650-663.

Ehlert, D., Horn, H.J. and Adamek, R. (2008). Measuring crop biomass density by laser triangulation. *Computers and Electronics in Agriculture* **61**: 117-125.

Erdle, K., Mistele, B. and Schmidhalter, U. (2013). Spectral high-throughput assessments of phenotypic differences in biomass and nitrogen partitioning during grain filling of wheat under high yielding Western European conditions. *Field Crops Research* **141**: 16-26.

Evans, G.C. (1972). The quantitative analysis of plant growth. Univ of California Press.

Fahlgren, N., Feldman, M., Gehan, M.A., Wilson, M.S., Shyu, C., Bryant, D.W., Hill, S.T., McEntee, C.J., Warnasooriya, S.N., Kumar, I. and Ficor, T. (2015). A versatile phenotyping system and analytics platform reveals diverse temporal responses to water availability in *Setaria*. *Molecular Plan* **8**: 1520-1535.

Fanourakis, D., Briese, C., Max, J.F., Kleinen, S., Putz, A., Fiorani, F., Ulbrich, A. and Schurr, U., (2014). Rapid determination of leaf area and plant height by using light curtain arrays in four species with contrasting shoot architecture. *Plant Methods* **10**: 9. DOI**:** 10.1186/1746-4811-10-9.

Feng, H., Jiang, N., Huang, C., Fang, W., Yang, W., Chen, G., Xiong, L. and Liu, Q. (2013). A hyperspectral imaging system for an accurate prediction of the above-ground biomass of individual rice plants. *Review of Scientific Instruments* **84**: 095107.

Fiorani, F. and Schurr, U. (2013). Future scenarios for plant phenotyping. *Annual Review of Plant Biology* **64***:* 267-291.

Fleming, G.M., Wunderle, J.M., Ewert, D.N. and O'Brien, J.J. (2014). Estimating plant biomass in early-successional subtropical vegetation using a visual obstruction technique. *Applied Vegetation Science* **17**: 356-366.

Flood, P.J., Kruijer, W., Schnabel, S.K., Schoor, R., Jalink, H., Snel, J.F., Harbinson, J. and Aarts, M.G. (2016). Phenomics for photosynthesis, growth and reflectance in *Arabidopsis thaliana* reveals circadian and long-term fluctuations in heritability. *Plant Methods* **12**: 14. DOI: 10.1186/s13007-016-0113-y.

Fricke, T. and Wachendorf, M. (2013). Combining ultrasonic sward height and spectral signatures to assess the biomass of legume–grass swards. *Computers and Electronics in Agriculture* **99**: 236-247.

Ganguli, A.C., Vermeire, L.T., Mitchell, R.B. and Wallace, M.C. (2000). Comparison of four nondestructive techniques for estimating standing crop in shortgrass plains. *Agronomy Journal* **92**: 1211-1215.

Gardner FP, Pearce RB and Mitchell RL (1985). Physiology of Crop Plants. pp. 327 pp. Iowa State University Press.

Garrigues, S., Shabanov, N.V., Swanson, K., Morisette, J.T., Baret, F. and Myneni, R.B. (2008). Intercomparison and sensitivity analysis of Leaf Area Index retrievals from LAI-2000, AccuPAR, and digital hemispherical photography over crop lands. *Agricultural and Forest Meteorology* **148**: 1193-1209.

Ghanem, M.E., Marrou, H. and Sinclair, T.R. (2015). Physiological phenotyping of plants for crop improvement. *Trends in Plant Science* **20**: 139-144.

Golzarian M. R., Frick, R. A., Rajendran, K., Berger, B., Roy, S., Tester, M. and Lun, D. S. (2011). Accurate inference of shoot biomass from high-throughput images of cereal plants. *Plant Methods* **7:** 1-11.

Gonsamo, A., Walter, J.M.N. and Pellikka, P. (2010). Sampling gap fraction and size for estimating leaf area and clumping indices from hemispherical photographs. *Canadian Journal of Forest Research* **40**: 1588-1603.

Gower, S.T. and Norman, J.M. (1991). Rapid estimation of leaf area index in forests using the LI-COR LAI-2000. *Ecology* **72**: 896-1.

Grieder C, Hund A and Walter A (2015). Image based phenotyping during winter: a powerful tool to assess wheat genetic variation in growth response to temperature. *Functional Plant Biology* **42:** 387-396.

Hairmansis, A., Berger, B., Tester, M. and Roy, S.J. (2014). Image-based phenotyping for non-destructive screening of different salinity tolerance traits in rice. *Rice* **7**: 16.

Harmoney, K.R., Moore, K.J., George, J.R., Brummer E.C. and Russell J.R. (1997). Determination of pasture biomass using four indirect methods. *Agronomy Journal* **89**: 665-672.

Hawkesford, M.J., Araus, J.L., Park, R., Calderini, D., Miralles, D., Shen, T., Zhang, J. and Parry, M.A. (2013). Prospects of doubling global wheat yields. *Food and Energy Security* **2**: 34-48.

Hiscox, J.T. and Israelstam, G.F. (1979). A method for the extraction of chlorophyll from leaf tissue without maceration. *Canadian Journal of Botany* **57**: 1332-1334.

Honsdorf, N., March, T.J., Berger, B., Tester, M. and Pillen, K. (2014). High-throughput phenotyping to detect drought tolerance QTL in wild barley introgression lines. *PLoS One* **9**: e97047. DOI: 10.1371/journal.pone.0097047.

Horgan, G.W., Song, Y., Glasbey, C.A., van der Heijden, G.W., Polder, G., Dieleman, J.A., Bink, M.C. and van Eeuwijk, F.A. (2015). Automated estimation of leaf area development in sweet pepper plants from image analysis. *Functional Plant Biology* **42**: 486-492.

Hoyos-Villegas, V., Houx, J.H., Singh, S.K. and Fritschi F.B. (2014). Ground-Based Digital Imaging as a Tool to Assess Soybean Growth and Yield. *Crop Science* **54**:1756-1768.

Humplík, J.F., Lazár, D., Fürst, T., Husičková, A., Hýbl, M. and Spíchal, L. (2015). Automated integrative high-throughput phenotyping of plant shoots: a case study of the cold-tolerance of pea (*Pisum sativum* L.). *Plant Methods* **11**: 20. **DOI:** 10.1186/s13007-015-0063-9

Hunt, C.L., Jones, C.S., Hickey, M.J., Koolaard, J.P., West, J. and Hatier, J.H.B. (2015). Estimation in the Field of Individual Perennial Ryegrass Plant Position and Dry Matter Production Using a Custom-Made High-Throughput Image Analysis Tool. *Crop Science* **55**: 2910-2917.

Jia, B., He, H., Ma, F., Diao, M., Jiang, G., Zheng, Z., Cui, J. and Fan, H. (2014). Use of a digital camera to monitor the growth and nitrogen status of cotton. *The Scientific World Journal* Article ID 602647. DOI: 10.1155/2014/602647.

Johnson P. S., Johnson C. L. & West N. E. (1998) Estimation of phytomass for ungrazed crested wheatgrass plants using allometric equations. *J. Range Manage* **41**: 421–5.

Johnson, M.D., Hsieh, W.W., Cannon, A.J., Davidson, A. and Bédard, F. (2016). Crop yield forecasting on the Canadian Prairies by remotely sensed vegetation indices and machine learning methods. *Agricultural and Forest Meteorology* **218**: 74-84.

Johnson, P. S., Johnson, C. L. and West N. E. (1998). Estimation of phytomass for ungrazed crested wheatgrass plants using allometric equations. *J. Range Manage* **41**: 421–5.

Jonckheere, I., Fleck, S., Nackaerts, K., Muys, B., Coppin, P., Weiss, M. and Baret, F. (2004). Review of methods for in situ leaf area index determination: Part I.

Theories, sensors and hemispherical photography. *Agricultural and Forest Meteorology* **121**: 19-35.

Junker, A., Muraya, M.M., Weigelt-Fischer, K., Arana-Ceballos, F., Klukas, C., Melchinger, A.E., Meyer, R.C., Riewe, D. and Altmann, T. (2014). Optimizing experimental procedures for quantitative evaluation of crop plant performance in high throughput phenotyping systems. *Frontiers in Plant Science* **5**: 770. 20 January 2015. DOI: 10.3389/fpls.2014.00770.

Kefauver, S.C., El-Haddad, G., Vergara-Diaz, O. and Araus, J.L. (2015), October. RGB picture vegetation indexes for High-Throughput Phenotyping Platforms (HTPPs). In: *SPIE Remote Sensing* (pp. 96370J-96370J). International Society for Optics and Photonics.

Kipp, S., Mistele, B., Baresel, P. and Schmidhalter, U. (2014). High-throughput phenotyping early plant vigour of winter wheat. *European Journal of Agronomy* **52**: 271-278.

Kirk, K., Andersen, H.J., Thomsen, A.G., Jørgensen, J.R. and Jørgensen, R.N. (2009). Estimation of leaf area index in cereal crops using red–green images. *Biosystems Engineering* **104**: 308-317.

Kjaer, K.H. and Ottosen, C.O. (2015). 3D laser triangulation for plant phenotyping in challenging environments. *Sensors* **15**: 13533-13547.

Klukas, C., Chen, D. and Pape, J.M., (2014). Integrated analysis platform: an open-source information system for high-throughput plant phenotyping. *Plant Physiology*. **165**: 506-518.

Koppe, W., Gnyp, M.L., Hennig, S.D., Li, F., Miao, Y., Chen, X., Jia, L. and Bareth, G. (2012). Multi-temporal hyperspectral and radar remote sensing for estimating winter wheat biomass in the North China Plain. *Photogrammetrie-Fernerkundung-Geoinformation* 2012: 281-298.

Le Dantec, V., Dufrêne, E. and Saugier, B. (2000). Interannual and spatial variation in maximum leaf area index of temperate deciduous stands. *Forest Ecology and Management* **134**: 71-81.

Lee, K.J. and Lee, B.W. (2013). Estimation of rice growth and nitrogen nutrition status using color digital camera image analysis. *European Journal of Agronomy* **48**: 57-65.

Leister, D., Varotto, C., Pesaresi, P., Niwergall, A. and Salamini, F. (1999). Large-scale evaluation of plant growth in *Arabidopsis thaliana* by non-invasive image analysis. *Plant Physiology and Biochemistry* **37**: 671-678.

LemnaTec GmbH Matthias Eberius Pascalstr. 59 52076 Aachen, Germany matthias.eberius@lemnatec.com www.lemnatec.com

Li, L., Zhang Q, Huang, D. (2014). A review of imaging techniques for plant phenotyping. *Sensors* **14:** 20078-20111.

Liebisch, F., Kirchgessner, N., Schneider, D., Walter, A. and Hund, A. (2015). Remote, aerial phenotyping of maize traits with a mobile multi-sensor approach. *Plant Methods* **11**: 9. DOI: 10.1186/s13007-015-0048-8.

Liebisch, F., Pfeifer, J., Khanna, R., Lottes, P., Stachniss, C., Falck, T., Sander, S., Siegwart, R., Walter, A. and Galceran, E. (2016). Flourish –A robotic approach for automation in crop management. 22. Workshop Computer-Bildanalyse und Unbemannte autonom fliegende Systeme in der Landwirtschaft 21.04.2016 in Wernigerode Hochschule Harz Fachbereich Automatisierung

Liu, J. and Pattey, E. (2010). Retrieval of leaf area index from top-of-canopy digital photography over agricultural crops. *Agricultural and Forest Meteorology* **150**: 1485-1490.

Liu, J., Pattey, E. and Admiral, S. (2013). Assessment of in situ crop LAI measurement using unidirectional view digital photography. *Agricultural and forest meteorology* **169**: 25-34.

Lootens, P., Ruttink, T., Rohde, A., Combes, D., Barre, P. and Ruiz, I.R. (2016). High throughput phenotyping of lateral expansion and regrowth of spaced *Lolium perenne* plants using on field image analysis. *Plant Methods* **12***:*32. DOI 10.1186/s13007-016-0132-8

Menzel, M.I., Tittmann, S., Buehler, J., Preis, S., Wolters, N., Jahnke, S., Walter, A., Chlubek, A., Leon, A., Hermes, N. and Offenhaeuser, A, (2009). Non-invasive determination of plant biomass with microwave resonators. *Plant, Cell & Environment* **32**: 368-379.

Mistele, B. and Schmidhalter, U. (2008). Spectral measurements of the total aerial N and biomass dry weight in maize using a quadrilateral-view optic. *Field Crops Research* **106**: 94-103.

Monsi, M. and Saeki, T. (1953). The light factor in plant communities and its significance for dry matter production. *Japanese Journal of Botany* **14**: 22-52.

Montes, J.M., Technow, F., Dhillon, B.S., Mauch, F. and Melchinger, A.E. (2011). High-throughput non-destructive biomass determination during early plant development in maize under field conditions. *Field Crops Research* **121**: 268-273.

Mullan, D. and Garcia, M.B. (2012). Crop ground cover. In: Pask, A.J.D., Pietragalla, J., Mullan, D.M. and Reynolds, M.P. (Eds.) *Physiological Breeding II*: *A Field Guide to Wheat Phenotyping*. Mexico, D.F. CIMMYT.

Mullan, D.J. and Reynolds, M.P. (2010). Quantifying genetic effects of ground cover on soil water evaporation using digital imaging. *Functional Plant Biology* **37**: 703–712.

Murray, S.C., Knox, L., Hartley, B., Méndez-Dorado, M.A., Richardson, G., Thomasson, J.A., Shi, Y., Rajan, N., Neely, H., Bagavathiannan, M. and Dong, X. (2016). High clearance phenotyping systems for season-long measurement of corn, sorghum and other row crops to complement unmanned aerial vehicle systems. In: *SPIE Commercial+ Scientific Sensing and Imaging* (pp. 986607-986607). International Society for Optics and Photonics.

Neilson, E.H., Edwards, A.M., Blomstedt, C.K., Berger, B., Møller, B.L. and Gleadow, R.M. (2015). Utilization of a high-throughput shoot imaging system to examine the dynamic phenotypic responses of a C4 cereal crop

plant to nitrogen and water deficiency over time. *Journal of Experimental Botany* **66**: 1817-1832.

Neumann, K., Klukas, C., Friedel, S., Rischbeck, P., Chen, D., Entzian, A., Stein, N., Graner, A. and Kilian, B. (2015). Dissecting spatiotemporal biomass accumulation in barley under different water regimes using high-throughput image analysis. *Plant, Cell & Environment* **38**: 1980-1996.

Nilson, T. (1971). A theoretical analysis of the frequency of gaps in plant stands. *Agricultural. Meteorology* **8**: 25–38.

Oliveras, I., Eynden, M., Malhi, Y., Cahuana, N., Menor, C., Zamora, F. and Haugaasen, T. (2014). Grass allometry and estimation of above-ground biomass in tropical alpine tussock grasslands. *Austral Ecology* **39**: 408-415.

Paloscia, S. and Pampaloni, P. (1992). Microwave vegetation indexes for detecting biomass and water conditions of agricultural crops. *Remote Sensing of Environment* **40**: 15-26.

Pantazi, X.E., Moshou, D., Alexandridis, T., Whetton, R.L. and Mouazen, A.M. (2016). Wheat yield prediction using machine learning and advanced sensing techniques. *Computers and Electronics in Agriculture* **121**: 57-65.

Parent, B., Shahinnia, F., Maphosa, L., Berger, B., Rabie, H., Chalmers, K., Kovalchuk, A., Langridge, P. and Fleury, D. (2015). Combining field performance with controlled environment plant imaging to identify the genetic control of growth and transpiration underlying yield response to water-deficit stress in wheat. *Journal of Experimental Botany* **66**: 5481-5492.

Paruelo, J.M., Lauenroth, W.K. and Roset, P.A. (2000). Estimating aboveground plant biomass using a photographic technique. *Journal of Range Management* **53**: 190-193.

Pauli, D., Andrade-Sanchez, P., Carmo-Silva, A.E., Gazave, E., French, A.N., Heun, J., Hunsaker, D.J., Lipka, A.E., Setter, T.L., Strand, R.J. and Thorp, K.R. (2016). Field-based high-throughput plant phenotyping reveals the temporal patterns of quantitative trait loci associated with stress-responsive traits in cotton. *Genes Genomes Genetics* **6**: 865-879.

Paulus, S., Schumann, H., Kuhlmann, H. and Léon, J. (2014). High-precision laser scanning system for capturing 3D plant architecture and analysing growth of cereal plants. *Biosystems Engineering* **121**: 1-11.

Pearson, R.L., Tucker, C.J. and Miller, L.D. (1976). Spectral mapping of shortgrass prairie biomass. *Photogrammetric Engineering and Remote Sensing* **42**: 317-323.

Prasad, B., Babar, M.A., Carver, B.F., Raun, W.R. and Klatt, A.R. (2009). Association of biomass production and canopy spectral reflectance indices in winter wheat. *Canadian Journal of Plant Science* **89**: 485-496.

Psomas, A., Kneubühler, M., Huber, S., Itten, K. and Zimmermann, N.E. (2011). Hyperspectral remote sensing for estimating aboveground biomass and for exploring species richness patterns of grassland habitats. *International Journal of Remote Sensing* **32**: 9007-9031.

Rasmussen, J., Ntakos, G., Nielsen, J., Svensgaard, J., Poulsen, R.N. and Christensen, S. (2016). Are vegetation indices derived from consumer-grade cameras mounted on UAVs sufficiently reliable for assessing experimental plots? *European Journal of Agronomy* **74**: 75-92.

Reddersen, B., Fricke, T. and Wachendorf, M. (2014). A multi-sensor approach for predicting biomass of extensively managed grassland. *Computers and Electronics in Agriculture* **109**: 247-260.

Reusch, S. (2009). Use of ultrasonic transducers for on-line biomass estimation in winter wheat. In: van Henten, E.J., Goense, D., Lokhorst, D. (Eds.), Proceedings Precision Agriculture ‘09. Wageningen Academic Publishers, pp. 169–175.

Reynolds, M., Foulkes, J., Furbank, R., Griffiths, S., King, J., Murchie, E., Parry, M. and Slafer, G. (2012). Achieving yield gains in wheat. *Plant, Cell and Environment* **35**: 1799-1823.

Rischbeck, P., Elsayed, S., Mistele, B., Barmeier, G., Heil, K. and Schmidhalter, U. (2016). Data fusion of spectral, thermal and canopy height parameters for

improved yield prediction of drought stressed spring barley. *European Journal of Agronomy* **78**: 44-59.

Robel, R.J., Briggs, J.N., Dayton, A.D. and Hulbert, L.C., 1970. Relationships between visual obstruction measurements and weight of grassland vegetation. *Journal of Range Management* **23**: 295-297.

Sakamoto, T., Gitelson, A.A., Nguy-Robertson, A.L., Arkebauer, T.J., Wardlow, B.D., Suyker, A.E., Verma, S.B. and Shibayama, M. (2012). An alternative method using digital cameras for continuous monitoring of crop status. *Agricultural and Forest Meteorology* **154**: 113-126.

Sanderson, M.A., Rotz, C.A., Fultz, S.W. and Rayburn E.B. (2001). Estimating forage mass with a commercial capacitance meter, rising plate meter, and pasture ruler. *Agronomy Journal* **93**:1281-1286.

Schaefer, M.T. and Lamb, D.W. (2016). A combination of plant NDVI and LiDAR measurements improve the estimation of pasture biomass in tall fescue (*Festuca arundinacea* var. Fletcher). *Remote Sensing* **8**: 109. DOI:10.3390/rs8020109

Schirrmann, M., Hamdorf, A., Garz, A., Ustyuzhanin, A. and Dammer, K.H. (2016). Estimating wheat biomass by combining image clustering with crop height. *Computers and Electronics in Agriculture* **121**: 374-384.

Serrano, L., Filella, I. and Penuelas, J. (2000). Remote sensing of biomass and yield of winter wheat under different nitrogen supplies. *Crop Science* **40**: 723-731.

Sharma, B. and Ritchie G.L. (2015). High-Throughput Phenotyping of Cotton in Multiple Irrigation Environments. *Crop Science* **55**: 958-969

Sharma-Natu, P. and Ghildiyal, M.C. (2005). Potential targets for improving photosynthesis and crop yield. *Current Science* **88**: 1918-1928.

Sieling, K., Böttcher, U. and Kage, H. (2016). Dry matter partitioning and canopy traits in wheat and barley under varying N supply. *European Journal of Agronomy* **74**: 1-8.

Sugiura, R., Tsuda, S., Tamiya, S., Itoh, A., Nishiwaki, K., Murakami, N., Shibuya, Y., Hirafuji, M. and Nuske, S. (2016). Field phenotyping system for the

assessment of potato late blight resistance using RGB imagery from an unmanned aerial vehicle. *Biosystems Engineering* **148**: 1-10.

Svensgaard, J., Roitsch, T. and Christensen, S. (2014). Development of a mobile multispectral imaging platform for precise field phenotyping. *Agronomy* **4**: 322-336.

Tackenberg O (2007). A new method for non-destructive measurement of biomass, growth rates, vertical biomass distribution and dry matter content based on digital image analysis. *Annals of Botany* **99**: 777-783.

Thoren, D. and Schmidhalter, U. (2009). Nitrogen status and biomass determination of oilseed rape by laser-induced chlorophyll fluorescence. *European Journal of Agronomy* **30**: 238-242.

Thorp, K.R., Gore, M.A., Andrade-Sanchez, P., Carmo-Silva, A.E., Welch, S.M., White, J.W. and French, A.N. (2015). Proximal hyperspectral sensing and data analysis approaches for field-based plant phenomics. *Computers and Electronics in Agriculture* **118**: 225-236.

Tilly, N., Hoffmeister, D., Cao, Q., Lenz-Wiedemann, V., Miao, Y. and Bareth, G. (2013). Precise plant height monitoring and biomass estimation with Terrestrial Laser Scanning in paddy rice. In; M. Scaioni, R.C. Lindenbergh, S. Oude Elberink, D. Schneider and F. Pirotti eds.,,Proceedings of the ISPRS Annals of the Photogrammetry, Remote Sensing and Spatial Information Sciences Conference, Antalya, Turkey (Vol. 1113).

Tomasel, F.G., Paruelo, J.M., Abras, G., Ballarin, V. and Moler, E. (2001). A chromaticity-based technique for estimation of above-ground plant biomass. *Applied Vegetation Science* **4**: 207-212.

Tucker, C.J., Holben, B.N., Elgin, J.H. and McMurtrey, J.E. (1981). Remote sensing of total dry-matter accumulation in winter wheat. *Remote Sensing of Environment* **11**: 171-189.

Vadez, V., Kholová, J., Hummel, G., Zhokhavets, U., Gupta, S.K. and Hash, C.T. (2015). LeasyScan: a novel concept combining 3D imaging and lysimetry for

high-throughput phenotyping of traits controlling plant water budget. *Journal of Experimental Botany* DOI:10.1093/jxb/erv251.

Van der Heijden, G., Song, Y., Horgan, G., Polder, G., Dieleman, A., Bink, M., Palloix, A., van Eeuwijk, F. and Glasbey, C. (2012). SPICY: towards automated phenotyping of large pepper plants in the greenhouse. *Functional Plant Biology* **39**: 870-877.

Van Gardingen, P.R., Jackson, G.E., Hernandez-Daumas, S., Russell, G. and Sharp, L. (1999). Leaf area index estimates obtained for clumped canopies using hemispherical photography. *Agricultural and Forest Meteorology* **94**: 243-257.

Walter, A., Scharr, H., Gilmer, F., Zierer, R., Nagel, K.A., Ernst, M., Wiese, A., Virnich, O., Christ, M.M., Uhlig, B. and Jünger, S. (2007). Dynamics of seedling growth acclimation towards altered light conditions can be quantified *via* GROWSCREEN: a setup and procedure designed for rapid optical phenotyping of different plant species. *New Phytologist* **174**: 447-455.

Wang, L.A., Zhou, X., Zhu, X., Dong, Z. and Guo, W. (2016). Estimation of biomass in wheat using random forest regression algorithm and remote sensing data. *The Crop Journal* **4**: 212-219.

Watson, D.J. (1947). Comparative physiological studies in the growth of field crops. I. Variation in net assimilation rate and leaf area between species and varieties, and within and between years. *Annals of Botany* **11**: 41–76.

Watson, D.J. (1952). The physiological basis of variation in yield. *Advances in Agronomy* **4**: 101-145.

Weber, V.S., Araus, J.L., Cairns, J.E., Sanchez, C., Melchinger, A.E. and Orsini, E. (2012). Prediction of grain yield using reflectance spectra of canopy and leaves in maize plants grown under different water regimes. *Field Crops Research* **128**: 82-90.

Weiner, J., Kinsman, S. and Williams, S. (1998). Modeling the growth of individuals in plant populations: local density variation in a strand population of

Xanthium strumarium (Asteraceae). *American Journal of Botany* **85**: 1638-1645.

Weiss, M., Baret, F., Smith, G.J., Jonckheere, I. and Coppin, P. (2004). Review of methods for in situ leaf area index (LAI) determination: Part II. Estimation of LAI, errors and sampling. *Agricultural and Forest Meteorology* **121**: 37-53.

Wellburn, A.R (1994). The spectral determination of chlorophylls a and b, as well as total carotenoids, using various solvents with spectrophotometers of different resolution. *Journal of Plant Physiology* **144**: 307-313.

Welles, J. M. (1990). Some indirect methods of estimating canopy structure. In: J. Norman and N. Goel (eds) Instrumentation for studying vegetation canopies for remote sensing in optical and thermal infrared regions. Harwood Academic Publishers GmbH, London.

Welles, J. M. and J. M. Norman (1991). Instrument for indirect measurement of canopy architecture. *Agronomy Journal* **83**: 818-825.

Welles, J.M. and Cohen, S. (1996). Canopy structure measurement by gap fraction analysis using commercial instrumentation. *Journal of Experimental Botany* **47**: 1335-1342.

White, J. W. and M. M. Conley (2013). A flexible, low-cost cart for proximal sensing. *Crop Science* **53**: 1646-1649

Williams, R.F. (1946). The physiology of plant growth with special reference to the concept of net assimilation rate. *Annals of Botany* **10**:.41-72.

Wilson, J.W. (1960). Inclined point quadrats. *New Phytologist* **59**: 1-7.

Wilson, J.W., (1963). Estimation of foliage denseness and foliage angle by inclined point quadrats. *Australian journal of botany* **11**: 95-105.

Winterhalter, L., Mistele, B. and Schmidhalter, U. (2013). Evaluation of active and passive sensor systems in the field to phenotype maize hybrids with high-throughput. *Field Crops Research* **154**: 236-245.

Yousfi, S., Kellas, N., Saidi, L., Benlakehal, Z., Chaou, L., Siad, D., Herda, F., Karrou, M., Vergara, O., Gracia, A. and Araus, J.L. (2016). Comparative

performance of remote sensing methods in assessing wheat performance under Mediterranean conditions. *Agricultural Water Management* **164**: 137-147.

Zack, G.W., Rogers, W.E. and Latt, S.A.(1977). Automatic measurement of sister chromatid exchange frequency. *Journal of Histochemistry and Cytochemistry* **25**: 741-753.

Zhou, L., Pan, G. and Shi, Z. (2010). Methodology comparison for effective LAI retrieving based on digital hemispherical photograph in rice canopy. In *International Conference on Computer and Computing Technologies in Agriculture* (pp. 71-82). Springer Berlin Heidelberg.